CZECH TECHNICAL
UNIVERSITY
IN PRAGUE

F3

Faculty of Electrical Engineering

Department of Electromagnetic Field

Master's Thesis

Phantom of Muscular Tissue Based on Agar

Michaela Kantová

Electronics and Communications - Radio and Optical Technology

January 2020

Supervisor: prof. Ing. Jan Vrba, CSc.

MASTER'S THESIS ASSIGNMENT

I. Personal and study details

Student's name: **Kantová Michaela** Personal ID number: **434851**

Faculty / Institute: **Faculty of Electrical Engineering**

Department / Institute: **Department of Electromagnetic Field**

Study program: **Electronics and Communications**

Branch of study: **Radio and Optical Technology**

II. Master's thesis details

Master's thesis title in English:

Phantom of Muscular Tissue Based on Agar

Master's thesis title in Czech:

Fantom svalové tkáně na bázi agaru

Guidelines:

Your task is to study the scientific literature on the design of phantoms of biological tissues for diagnostic and therapeutic applications of microwave technologies in medicine. Phantom should imitate dielectric parameters of muscle in the band 200 - 3000 MHz. Learn the methods for measuring the complex permittivity of materials and then choose a methodology suitable for measuring the complex permittivity of biological tissues.
In the frame of this thesis, design and realize a new type of phantom of muscle tissue (based on agar with high water content) usable for testing microwave imaging and hyperthermia systems. Phantom should imitate dielectric parameters of muscle in the band 200 - 3000 MHz. Measure and evaluate dielectric parameters. Next, verify the time stability of this phantom in the laboratory.

Bibliography / sources:

[1] Vrba, J.: „Lékařské aplikace mikrovlnné techniky". Skriptum ČVUT-FEL, Praha, 2007
[2] Vrbajr, J.: „ Perspective medical diagnostics methods based on microwave measurement of dielectric properties of biological tissues". Habilitační práce ČVUT-FBMI, Kladno, 2017
[3] Vrba, D.: "Perspective use of MTM applicators in clinical practise". Habilitační práce ČVUT-FBMI, Kladno, 2018
[4] Fišer, O.: „Microwave hyperthermia for treatment of head and neck tumors controlled by non-invasive temperature monitoring based on UWB radar". Disertační práce ČVUT-FEL, Praha, 2018

Name and workplace of master's thesis supervisor:

prof. Ing. Jan Vrba, CSc., Department of Electromagnetic Field, FEE

Name and workplace of second master's thesis supervisor or consultant:

Date of master's thesis assignment: **09.10.2018** Deadline for master's thesis submission: **07.01.2020**

Assignment valid until:
by the end of winter semester 2020/2021

prof. Ing. Jan Vrba, CSc. Supervisor's signature	Head of department's signature	prof. Ing. Pavel Ripka, CSc. Dean's signature

Acknowledgement / Declaration

I would like to thank my master's thesis supervisor prof. Ing. Jan Vrba, CSc. who introduced me to biomedical applications of electromagnetic fields and assisted me and inspired me with his remarks. I also want to express my gratitude to Ing. Ondřej Fišer, PhD. for long-term cooperation and patient guidance through the whole design and measurement process.

Furthermore, I would like to thank my parents, who have always supported and encouraged me during my university studies.

I hereby declare that this thesis is my own work, and I cited all sources in accordance with Methodical Guidelines on Adherence to Ethical Policy during Higher Education Thesis Preparation.

Prohlašuji, že jsem předloženou práci vypracovala samostatně a uvedla jsem veškeré použité informační zdroje v souladu s Metodickým pokynem o dodržování etických principů při přípravě vysokoškolských závěrečných prací.

Prague, 6. 1. 2020

.....

Michaela Kantová

Abstrakt / Abstract

Cílem této diplomové práce je návrh a ověření fantomu na bázi agaru, který imituje vlastnosti svalové tkáně v mikrovlnném frekvenčním pásmu do 3 GHz. První část se zabývá fyzikálním principem dielektrických vlastností materiálu a jejich měřením. Materiály imitující biologické tkáně navržené v dostupné literatuře jsou diskutovány se zvláštním důrazem na fantomy založené na agaru. Celý proces návrhu je do detailu popsán společně s vyhodnocením naměřených výsledků a přípravou fantomu. Postup teplotně závislého měření je navržen pro dosažení vyšší přesnosti měření relativní permitivity a elektrické vodivosti. Na závěr byla použita Levenberg-Marquardtova metoda pro určení teplotně závislého Cole-Cole modelu fantomu.

Klíčová slova: hypertermie; imitace tkáně; svalový fantom; UWB radar, dielektrické vlastnosti.

Překlad titulu: Fantom svalové tkáně na bázi agaru

The goal of this master's thesis is to develop and verify a muscle-mimicking phantom at microwave frequencies up to 3 GHz. First, the physical principle of the material's dielectric properties and measurements is explained. Tissue mimicking materials which are proposed in the available literature are discussed and particular attention is paid to those that discuss phantoms based on agar. The complete design flow is described in detail as well as the measurement evaluation and the phantom fabrication process. A temperature measurement procedure is suggested to achieve higher accuracy in complex relative permittivity and electrical conductivity. Finally, the Levenberg-Marquardt method was used to determine a temperature-dependent Cole-Cole model for the proposed phatom.

Keywords: hyperthermia; tissue-mimicking; muscle phantom; UWB radar; dielectric properties.

/ Contents

Tables / Figures

Chapter 1
Introduction

The boom of biotechnology results in a growing interest in the possibilities of testing, calibrating and standardization of various medical devices. Tissue-mimicking materials (i.e. phantoms) are convenient materials for such biotechnological applications because they accurately represent dielectric and other properties which are particularly found in biological tissue and can offer an alternative to *ex vivo* bio-tissues whose properties decompose rapidly after being harvested. Such phantoms are essential for testing and optimising designed microwave imaging or hyperthermia systems.

Nowadays, cancer treatment is one of the greatest challenges of science. In 2016, cancer caused 1.7 million deaths worldwide and was the sixth global cause of death of that year [1]. However, in high-income countries cancer is the fourth cause of death. Cancer is the second cause of death in the Czech republic, specifically 27.0% men's and 22.3% woman's death were caused by cancer [2]. Hyperthermia (also called thermotherapy) is a complementary treatment technique with benefits for the patient such as lower radiotherapy dose and higher survival rate. The principle of hyperthermia is based on selectively killing the cancer cells by heating them and the effectiveness of the treatment depends heavily on the temperature which is achieved during the treatment. Temperature higher than 41 °C leads to cancer cell apoptosis (programmed cell death), whereas, normal cells can survive temperatures up to 45 °C. The goal of hyperthermia is to heat the tumour whithin the temperature range that ensures cancer cell apoptosis and the survival of normal cells. Reliable temperature monitoring is necessary to ensure the correct heating. Magnetic resonance thermometry is an example of such non-invasive temperature measurement method [3]. Nowadays several microwave technologies are studied for purpose of noninvasive monitoring of temperature or temperature change, e.g. UWB radar (which is investigated in the ref.[4]), microwave radiometers and microwave differential tomography. The goal of this thesis is to develop a phantom for testing novel UWB radar thermometry as well as various imaging and hyperthermia systems which could improve the medical care.

This work is focused on developing high-water content muscle mimicking phantom based on agar powder, which is intended for diagnostic and therapeutic applications of microwave imaging and hyperthermia systems in medicine. The gel form of the material was chosen for the research due to its capability to insert intracavitary and interstitial systems as well as testing surface systems. Such applications are one of the interests of the research team along with microwave imaging. The goal is to design phantom, which represents the dielectric properties on a frequency range from 200 MHz to 3000 MHz. The aim was to design a phantom with simple preparation, which does not require any special equipment and the substances are non-toxic.

The dielectric properties of interest were described for understanding their physical background. The first step of the phantom design was to carry out a detailed research about tissue-mimicking materials intended for microwave systems from available sources on the topic; the proposed phantoms are usually divided according to their form and also by the frequency band for the particular application. More details are discussed about gelatin phantom and specifically agar phantoms, which were chosen for design in this work. In the next chapter are described dielectric properties of materials in general and the workflow of designing of the phantom is presented with many measured data and comments. An essential part of the design is to develop the most suitable fabrication and preservation protocol procedure. Measuring dielectric parameters is a very complex issue with many problems and influences that can affect the measurement accuracy. A measurement with temperature-dependent calibration was performed and studied to improve performance accuracy. Different methods of measuring complex permittivity are discussed, and the best option according to our results is chosen for verification of dielectric properties. Several measurements over one week were performed for obtaining also long-term stability of the phantom properties. Temperature dependence of the phantom was observed over the temperature range of 25 °C - 50 °C. Finally, the evaluation of proposed phantoms along with its figures is presented. Temperature-dependent Cole-Cole model of phantom was estimated and verified.

The results of this work were successfully presented as the contributions [5],[6] on the conferences IUPESM 2018 and EuMCE 2019. Furthermore, the article was accepted in the International Journal of Microwave and Wireless Technologies.

Chapter 2
Physical Background

First of all, it is important to understand the physical background of the parameters of dielectric material that are in the main focus when designing tissue-mimicking phantom. Matter interaction with electromagnetic (EM) field can be described by the macroscopic parameters – complex relative permittivity, electrical conductivity and magnetic permeability. Their definition is based on Maxwell's equations which describe the EM field [3, 7]:

$$rot\boldsymbol{H} = \frac{\partial \boldsymbol{D}}{\partial t} + \boldsymbol{J_v} \tag{2.1}$$

$$rot\boldsymbol{E} = -\frac{\partial \boldsymbol{B}}{\partial \boldsymbol{t}} \tag{2.2}$$

$$div\boldsymbol{D} = \rho \tag{2.3}$$

$$rot\boldsymbol{B} = 0 \tag{2.4}$$

Relations between quantities for the inhomogeneous linear medium are described by so-called material equations [3]:

$$\boldsymbol{D} = \varepsilon \boldsymbol{E} \tag{2.5}$$

$$\boldsymbol{B} = \mu \boldsymbol{H} \tag{2.6}$$

$$\boldsymbol{J_v} = \boldsymbol{J} + \sigma \boldsymbol{E} \tag{2.7}$$

The meaning of all symbols and abbreviations is explained in appendix A. The material parameters are generally tensors that dependend on the frequency, temperature, position, magnitude and direction of the electric and magnetic intensity of the applied field. According to the behaviour to applied EM field are materials referred to as [8]:

- Linear – Parameters ε, μ and σ are not function of a field; otherwise they are called *nonlinear*. When a certain value is exceeded, the material starts to be non-linear (a typical example of such material is the air whose limit is $1 \cdot 10^6$ V/m).
- Homogeneous – Constitutive parameters are not position dependent. Their opposites are not so common *nonhomogeneous* materials.
- Nondispersive – Material parameters are frequency independent. In case of their frequency dependence, observed material is defined as *dispersive*. In reality, almost every material does show some degree of dispersion.
- Isotropic – Parameters are not the function of the direction of the applied field. An example of *anisotropic* material are crystals as they exhibit a high degree of anisotropy.

The physical principle of material interaction with EM field is based on the response of particles with an electric charge to the external field. This interaction results in the material's ability to store electric energy by shifting against the stationary state (analogous to potential energy in mechanics). The polarization of dielectrics is a complex physical process, which consists mainly of these mechanisms [8–9]:

- Electronic – the external electric field is applied, and the electron shell is biased relative to the nucleus
- Molecular (atomic) – the displacement of atoms due to the uneven distribution of the charge in the molecule
- Ionic – the molecules consist of positive and negative ions which are bound together by electric forces when applying external field, the positive ones are shifted out in the direction of field intensity, while negative in the opposite direction.
- Orientation (dipolar) – permanent dipoles are formed by the asymmetric distribution of opposite charge in the molecules of the substance

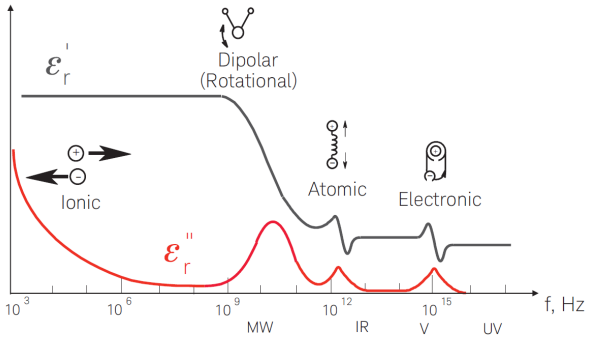

Figure 2.1. Frequency dependence of dielectric mechanisms. Taken from [10].

All these mechanisms result in a formation of an *elemental dipole*. Macroscopic scale model of this phenomenom is defined by electric polarization vector which can be explained as the dipole moment per volume. The total dipole moment of material is [8]:

$$\boldsymbol{p_t} = \sum_{n=1}^{\Delta v N_e} d\boldsymbol{p_i} \tag{2.8}$$

Where Δv is a volume and N_e represents number of electric dipoles per unit volume. Vector of electric polarization which has the same direction as the vector of applied field is then:

$$\boldsymbol{P} = \lim_{\Delta v \to 0} \left[\frac{1}{\Delta v} \boldsymbol{p_t} \right] \tag{2.9}$$

The dielectric material is an electrical insulator because there are no free electric charges since dominant charges of its atom structure are bound by atomic and molecular forces. Atoms and molecules appear neutral from a macroscopic point of view ($\boldsymbol{P} = 0$). Dielectrics are often divided into two main groups according to their charge distribution:

- Polar dielectrics – Polar materials' charges are distributed in such a way that in the absence of applied field the individual dipoles are formed but the net total dipole moment is zero as well as electric polarization vector. An example of this material is water. The mechanism is demonstrated in Fig. 2.2.
- Nonpolar dielectrics – Averaged nonpolar materials' charge cancel each other throughout the whole volume, no individual dipoles are formed and the total dipole moment, as well as electric polarization vector, are zeros. Oxygen is one such material. Illustrated in Fig. 2.3.

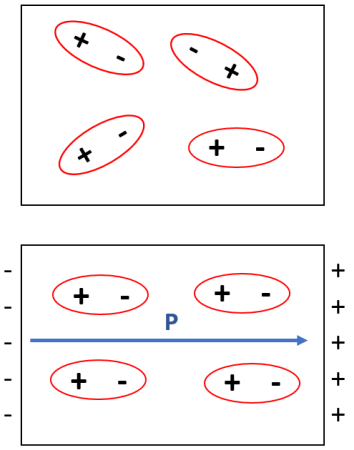

Figure 2.2. Polar dielectrics behaviour before and after applying external EM field.

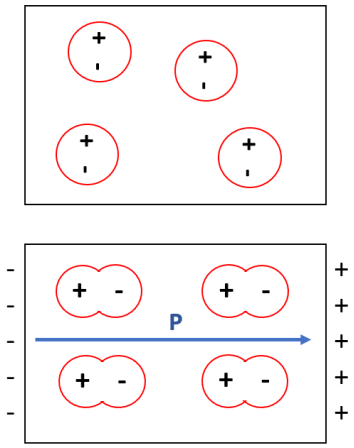

Figure 2.3. Nonpolar dielectrics behaviour before and after applying external EM field.

The electric displacement field is [8]:

$$\boldsymbol{D} = \varepsilon_0 \boldsymbol{E_a} + \boldsymbol{P} \tag{2.10}$$

Which can be simplified to the following form where ε_s is parameter in farads/meter.

$$\boldsymbol{D} = \varepsilon_s \boldsymbol{E_a} \tag{2.11}$$

For a linear, homogeneous, isotropic dielectric is $\boldsymbol{P}$ linearly dependend on applied field (expressed by two previous equations):

$$\boldsymbol{P} = \varepsilon_0 \varkappa_e \boldsymbol{E_a} \tag{2.12}$$

The electrical susceptibility $\varkappa_e$ indicates the measure of easiness to polarize the dielectric; and can be described by the permittivity of the material [8–9].

$$\varkappa_e = \frac{1}{\varepsilon_0} \frac{P}{E_a} \tag{2.13}$$

Electric flux density could be obtained by combining formulas mentioned above.

$$\boldsymbol{D} = \varepsilon_0 \boldsymbol{E_a} + \varepsilon_0 \varkappa_e \boldsymbol{E_a} = \varepsilon_0 (1 + \varkappa_e) \boldsymbol{E_a} = \varepsilon_s \boldsymbol{E_a} \tag{2.14}$$

From which relative value (compared to free space) of permittivity is described:

$$\varepsilon_{sr} = \frac{\varepsilon_s}{\varepsilon_0} = 1 + \varkappa_e \tag{2.15}$$

Where ε_s is static permittivity. Relative permittivity is also referred to as *dielectric constant*. The equation (2.15) implies that electric susceptibility of the vacuum is zero.

Relative permittivity of dielectric material indicates relative charge (energy) storage capabilities in comparison to free space. Air has relative permittivity close to one; water has among the highest relative permittivity which equals to 81 at static frequencies. The higher the value is, the greater storage capabilities the material has, thus the water has very high charge storage properties. This principle is also used in capacitors [8].

The second fundamental electric material parameter which will be explored is *conductivity*. Conductors are materials whose structure consists of a large number of valence (outer shell) electrons which are bounded very weakly to the atomic structure. Such electrons can migrate from one atom to another and are called *free electrons*. Free electron movement is random with different velocities in case of no presence of external field and produce zero net current through the surface of the conductor. When the external electric field is applied to conductor, the electrons still move randomly but slowly drift with velocity v_e in the negative direction to the applied field. This drift creates conduction current in the conductor. The electron velocity is proportional to applied field as [8–9]:

$$\boldsymbol{v_e} = \mu_e \boldsymbol{E} \tag{2.16}$$

Where μ_e is electron mobility. Current density may be expressed in the following form with q_{ve} electron charge density :

$$\boldsymbol{J} = q_{ve}\boldsymbol{v_e} = q_{ve}(-\mu_e \boldsymbol{E}) = -q_{ve}\mu_e \boldsymbol{E} \tag{2.17}$$

The proportional dependency of current density to the external electric field is expressed as well-known *Ohm's law* [9]:

$$\boldsymbol{J} = \sigma_s \boldsymbol{E} \tag{2.18}$$

Static conductivity in S/m is then defined as:

$$\sigma_s = -q_{ve}\mu_e \tag{2.19}$$

Static conductivity describes conductive properties of a material. The reciprocal value is called resistivity and has strong temperature dependence. Probability of collision between the free electrons increases with temperature, thus the conductivity of conductor decreases. Dielectrics have very low conductivity, which is ideally zero.

The relative static permittivity and static conductivity expressed above represents material behaviour when the external field is DC. However, when the applied field is alternating in polarity, the polarization vector $\boldsymbol{P}$ becomes the function of the external field frequency. Simultaneously incremental changes in the conductivity are reversed in polarity to an alternating field [8].

When the external field is applied, positive charges remain in a stationary position. However, negative charges move relative to the nucleus in accordance with the field. This phenomenon is possible to depict as a *spring–mass system*, known from Newtonian mechanics. Complex permittivity reflects the fact that the material's polarization is the function of angular frequency. When taking into consideration complex character then eq. (2.14) can be rewritten as:

$$De^{j\omega t} = \varepsilon^*(\omega) E_a e^{j\omega t} \tag{2.20}$$

D and E represents magnitudes of displacement and electric field, j is imaginary unit $j^2 = -1$ and $\omega = 2\pi \cdot frequency$.

$$\varepsilon^* = \varepsilon_0 + \frac{De^{j\omega t}}{E_a e^{j\omega t}} = \varepsilon' - j\varepsilon'' \tag{2.21}$$

This form is also reffered as *dispersion equation*. Lossy material is described by complex relative permittivity [3, 8]:

$$\varepsilon_r^* = \frac{\varepsilon^*}{\varepsilon_0} = \varepsilon_r' - j\varepsilon_r'' \tag{2.22}$$

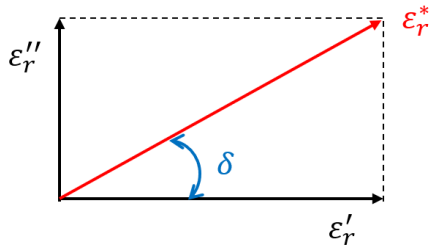

Figure 2.4. Complex permittivity and loss factor (angle) displayed in the form of simple vector diagram.

Where ε' is a real part of complex permittivity and represents the amounth of energy from external electric field that can be stored in material. The imaginary part of the complex permittivity called loss factor represents the loss in dielectric due to attenuation caused by dipole oscillations. Maxwell-Ampere eq. (2.1) can be rewritten using complex permittivity as:

$$rot\boldsymbol{H} = \boldsymbol{J_i} + \boldsymbol{J_c} + j\omega\varepsilon^*\boldsymbol{E} \tag{2.23}$$

Following form can be obtained after few more derivation steps:

$$rot\boldsymbol{H} = \boldsymbol{J_i} + \sigma_e\boldsymbol{E} + j\omega\varepsilon'\boldsymbol{E} \tag{2.24}$$

Where $\boldsymbol{J_i}$ is source electric current density, $\boldsymbol{J_c}$ is conduction electric current density. Equivalent (total) conductivity is defined:

$$\sigma_e = \sigma_s + \omega\varepsilon'' = \sigma_s + \sigma_a \tag{2.25}$$

It consists of static conductivity σ_s and alternating field conductivity σ_a. The alternating part is caused by the dipoles rotation, as the field is changing polarity, the phenomenon is called dielectric hysteresis. This principle causes heating of the material by using microwaves, and it is used in hyperthermia as well as in microwave ovens [8].

Tangent $\tan\delta$ is alternating electric *loss factor* that includes the effect of both dielectric and conductivity losses. Relations between complex permittivity and loss factor are illustrated in Fig. 2.4 and described in eq.(2.26).

$$\tan\delta_a = \frac{\sigma_a}{\omega\varepsilon'} = \frac{\varepsilon''}{\varepsilon'} \tag{2.26}$$

2.1 Cole-Cole Model

Permittivity and conductivity properties are for most materials frequency-dependent and consequently have a response to a current or voltage step. An exponential form can be considered as one of the simpliest response [11]:

$$1 - \exp(\frac{-t}{\tau}) \tag{2.27}$$

Relative permittivity changes are somehow proportional to variations of electric susceptibility. The imaginary part of the complex permittivity reaches the highest values at resonant frequencies (multiple resonant frequencies of oscillations throughout the spectrum). This phenomenom indicates that the material is in the most lossy state at those particular frequencies. The relation between the real and imaginary part of complex permittivity is expressed in *Kramers–Kronig relations* (similar relations as resistance and reactance in circuit theory) which shows that ε' and ε'' are conjugate functions. Materials with relaxation time can be modelled by the well-known *Debye equation*. The relation characterises the complex permittivity as a variation on frequency provided that real part of ε^* is known at zero frequency ε'_{rs} and also at infinite frequency $\varepsilon'_{r\infty}$ (ideally). For simple time response [8, 10, 12]:

$$\varepsilon^*_r(\omega) = \varepsilon'_r(\omega) - j\varepsilon''_r(\omega) = \varepsilon'_{r,\infty} + \frac{\varepsilon'_{r,s} - \varepsilon'_{r\infty}}{1 + j\omega\tau_{e,m}} \tag{2.28}$$

If the response is more complex in time domain, then the relation becomes a sum of exponentials:

$$\varepsilon^*_r(\omega) = \varepsilon'_{r,\infty} + \sum_{m=1}^{N} \frac{\varepsilon'_{r,s} - \varepsilon'_{r,\infty}}{1 + j\omega\tau_e} \tag{2.29}$$

The important material parameter is *relaxation time* τ, which is a measure of the mobility of the material's molecules [12].

$$\tau = \frac{\varepsilon}{\sigma} \tag{2.30}$$

A new relaxation time constant is introduced in Debye's equation, and is related to the original one as:

$$\tau_e = \tau \frac{\varepsilon'_{r,s} + 2}{\varepsilon'_{r,\infty} + 2} \tag{2.31}$$

The changes of the electric field at the frequencies below relaxation are slow enough to ensure that dipoles can keep pace with the field variations. The polarization can develop fully, so ε''_r is directly proportional to the frequency. The ε''_r increases and ε'_r begins to decrease because of phase lag between the dipole alignment and electric field at higher frequencies. On the other hand, above the relaxation frequency, the electric field is too fast, so the dipoles are not able to keep pace, and the dipole rotational, and orientation polarization disappears. Relative complex permittivity can also be represented in a *Cole–Cole diagram*, which is similar to the Smith chart and has ε'' and ε' on the vertical axis and frequency on the horizontal axis [8, 10].

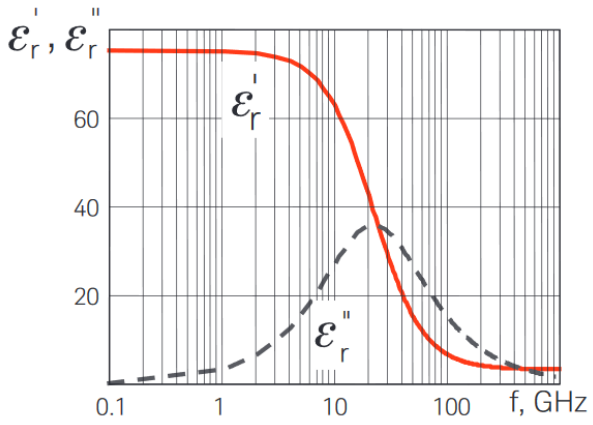

Figure 2.5. An example of Debye relaxation of the water at the temperature 30°. Taken from [10].

Another convenient representation of dispersion is in the complex plane locus (Argand diagram) in which complex part of relative permittivity is plotted against the real part. Each point corresponds to one frequency of measurement. The locus is a semicircle with its centre on the real part ε', the interception points for Debye model are ε_0 and ε_∞ [12]. Comparison of the Cole-Cole model with Debye equation is shown in the Fig. 2.6.

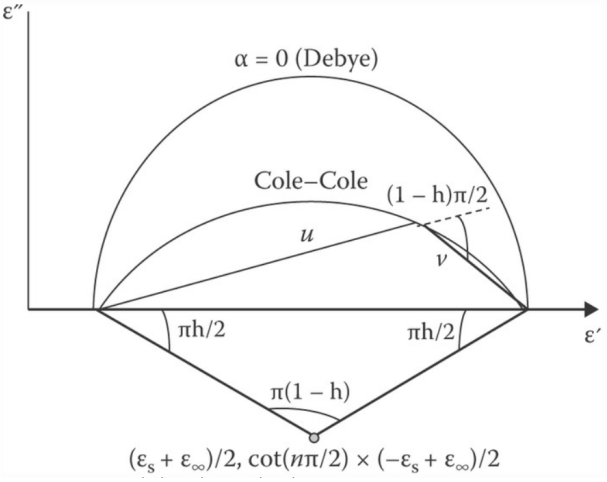

Figure 2.6. Representation of Cole-Cole and Debye models in complex plane. Taken from [13].

Kenneth S. Cole and Robert H. Cole showed that Debye's equation is not adequate dispersion description for the general matter. They build their new approach on experimental evidence which showed that the dispersion behaviour is actually present in the broader frequency range and the maximum value of the imaginary part of the dielectric constant is smaller than was originally supposed. Debye's equation assumes only dipole polarization; however, measured data denotes that polarization and absorption are due to several types of polarization. This difference is especially evident for liquid and solid dielectrics. New variable – index α was introduced into the original equation (2.28) to improve the description of frequency dependence. Index α can attain the value between 0 and 1. The lower the value of exponent $(1 - \alpha)$ is, the broader the relaxation time distribution becomes. Subsequently, the peak of the imaginary part becomes wider [12, 14].

N-pole Cole-Cole model for a lossy medium is defined as:

$$\varepsilon_r^*(\omega) = \varepsilon'_{r,\infty} + \sum_{m=1}^{N} \frac{\Delta\varepsilon_m}{(1 + j\omega\tau_{e,m})^{(1-\alpha_m)}} + \frac{\sigma}{j\omega\varepsilon_0} \tag{2.32}$$

Where commonly $\varepsilon'_{r,s} - \varepsilon'_{r,\infty} = \Delta\varepsilon$. Cole-Cole model is typically used for representing dielectric properties of biological tissues dependent on frequency. Gabriel et al. [15] is usually cited as a reference that summarizes parameters of four-pole Cole-Cole model of various biological tissues. It is also possible to generalize the expression for temperature dependence. All the variables are then dependent on the temperature as shown for example in [16]. The definition of the model dependent on temperature δ is then as follows:

$$\varepsilon_r^*(\omega, \delta) = \varepsilon'_{r,\infty}(\delta) + \sum_{m=1}^{N} \frac{\Delta\varepsilon_m(\delta)}{(1 + j\omega\tau_{e,m}(\delta))^{(1-\alpha_m)}} + \frac{\sigma(\delta)}{j\omega\varepsilon_0} \tag{2.33}$$

Debye and Cole-Cole relaxation models are not the only models used for describing a material. There is also the Davidson-Cole model which introduces another empirical parameter β. Studies showed that the Debye model is accurate for representing water dielectric properties, whereas Davidson-Cole model is an appropriate model for instance for ethanediol. Overall, these models are convenient in practice because they enable to calculate complex relative permittivity and conductivity with appropriate accuracy and computation complexity with just a few parameters [17].

The muscle tissue exhibits at least three major relaxation mechanisms called α, β and γ. Center frequencies are 80 Hz, 50 kHz and 25 GHz respectively at the human body temperature. The β dispersion can be described by the Cole-Cole function. At MW frequencies above 1 GHz up to 20 GHz tissue conductivity increases quadratically with the frequency which is caused mainly by its high-water content. On the other way around the permittivity is slowly decreasing with frequency. Figure 2.7 shows the permittivity as a function of frequency with those mechanisms [11].

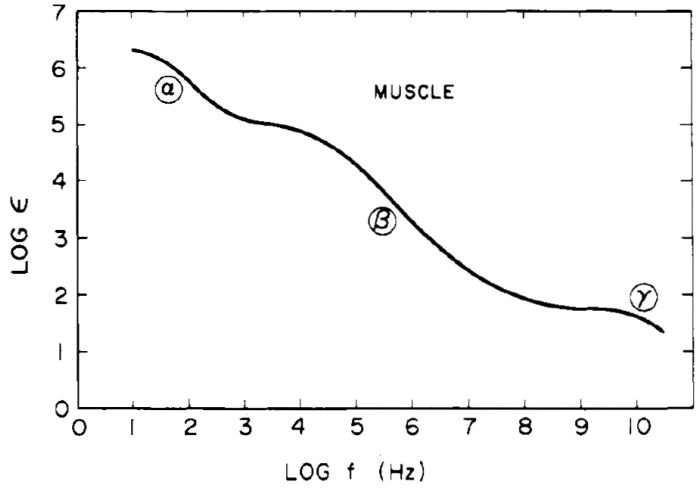

Figure 2.7. Frequency dependence of dielectric constant of muscle tissue with denoted three main relaxation mechanism's regions. Taken from [11].

The temperature coefficient is related to the relaxation mechanisms and describes temperature dependence. It is defined in proximity of characteristic frequency as [11]:

$$\frac{d\varepsilon}{\varepsilon} = \frac{d\sigma}{\sigma}\frac{\varepsilon_0 - \varepsilon_\infty}{\varepsilon_0 + \varepsilon_\infty} \tag{2.34}$$

where $\frac{d\varepsilon}{\varepsilon}$ is the relative change of dielectric constant as a consequence of the relative change of conductivity $\frac{d\sigma}{\sigma}$. Constants ε_0 and ε_∞ are moderately temperature independent and ε_0 is always higher than ε_∞. For biological tissues at MW frequencies varies permittivity temperature coefficient from 1 to 2; the conductivity temperature coefficient varies from -0.3 to 2. Each of the relaxation regions have a small negative dielectric constant with negative temperature coefficient at low and high frequencies and a positive coefficient in between [11].

- α dispersion – Mostly caused by ionic polarization, the temperature coefficient is equal to the conductivity of electrolyte so about 2 percent/ °C.
- β dispersion – This relaxation range is mainly caused by Maxwell-Wagner polarization effects. Cellular membrane's charging time constant is inversely proportional to conductivity of the electrolyte so temperature coefficient is also about 2 percent/ °C.
- γ dispersion – Relaxation is very close to the one of water so the temperature dependence is equal to the one of water which is close to 2 percent/ °C.

Chapter 3
Tissue-Mimicking Phantoms

The first step of designing a phantom was detailed literature research focused on the tissue-mimicking material at MW frequencies. Many different phantoms in many states for various applications were described in the literature to simulate dielectric properties of biological tissue. However, there is currently no full human body phantom for all frequency bands and all applications that could be used for testing novel systems. One of the main designing difficulties is the large diversity of soft human tissue dielectric properties over the frequencies and importance of mimicking exactness.

Ideally, a phantom should accurately represent all properties of the biological tissue, that are geometric, thermal, electrical, acoustic and optical properties, over a wide frequency and temperature ranges. However, such a model has not yet been created; each phantom varies according to the desired application. In addition to the properties mentioned above, phantom is also defined by its mechanical properties, the melting point, durability, ease of preparation and its price. Phantoms are used for testing and calibrating because they allow verification under the same conditions. Phantoms are classified into many groups, as is shown in the following part. The basic division is due to the form [18]:

- Liquid
- Solid
- Gel – the most popular ones because of their convenient mechanical properties

Phantoms are divided into two basic groups by the water content according to biological tissue which properties they mimic. Each of them has a specific composition of substances.

- High water content – muscle, brain, skin, internal organs
- Low water content – bones, fat

Since the human body is made of compositions of these tissues, phantoms can be designed as:

- Homogenous – mimic only one particular tissue (for example fat)
- Heterogenous – mimic part of the body (for example breast)

The aim of the scientific effort is to design a composition that mimics biological tissue within a wide frequency range and is anatomically realistic. Designing a phantom that meets the properties in the whole frequency range has not yet been successful. Phantoms are usually designed for certain frequency range, therefore mimic different properties [18].

- Ultrasound – 2 MHz to 15 MHz
- Optical – 400 THz to 700 THz (visible light)
- Microwave – 300 MHz to 300 GHz

Many phantoms mimicking diverse tissues are available commercially. The products are generally constructed for specific applications such as phantom with built-in sensors for measurement of MRI-induced fields or head phantom for hyperthermia applicator array or anthropomorphic phantom for testing mammographic system. Variety of phantoms is offered for example by IT'IS Foundation [19], CIRS [1] or NITS. [2] Commercial solutions are typically expensive and non-customizable, which is not convenient especially for research purposes. The price varies from hundreds to thousands of dollars [20].

3.1 Liquid Phantoms

Liquid phantoms are the simplest and the cheapest tissue-mimicking materials and are typically used to mimic the properties of blood. Their properties can be easily changed by changing the solution's compositions. The disadvantage may be short-time stability due to microbial degradation. The mixtures also tend to have sediments in the bottom of the container. The container defines their shape. Liquid phantoms are usually based on aqueous solutions involving saline or even also oily components [21]. Oil-in-water solutions usually mimic fat and bone tissue. Another possibility is to mix TX-100 with salted water.

Solutions based on glycerol or glycerin and water are used for ultrasound applications. Another recipe suggests to use machine cutting fluid with distilled water; the advantage is viscosity close to human blood [20]. Novel recipe based on egg white intended as blood coagulation surrogate is presented in [22].

3.2 Solid Phantoms

Solid phantoms exhibit long-time stability, durability and the easiness of transport. Their price is usually higher compared to liquid phantoms due to more complex fabrication requiring heating, cooling or hardening. They are usually divided into two groups according to the main ingredient – water-based and oil-based. Some of the perspective phantoms are described further.

A solid phantom consisting of graphite, carbon black and urethane rubber mimicking soft tissues from 1 to 10 GHz is presented in the article [23]. The choice of rubber was explored, however, urethane-based samples occurred to be more flexible, mechanically strong and have easier mixing process compared to silicone-based ones. Carbon black provides greater conductivity than graphite but has lower mixing limit, therefore, a combination of graphite and carbon black appeared to be the best. Specific dielectric properties are obtained by changing the concentration of carbon powder. The advantage of the fabrication is its easiness. Many other phantoms are based on this composition. The phantom was then enhanced to create breast phantom with a durable skin layer in [24]. Skin layer, fatty layer and glandular structures and tumours were prepared from carbon/rubber materials. The phantom exhibits similar reflections to human tissue, thus can be used for testing imaging algorithms. Variation of the above composition was also used to mimic the human head in [21] intended for testing EIT medical applications. The phantom is highly accurate in terms of AC conductivity in the frequency range 1 kHz -1 MHz.

[1] CIRS – Computerized Imaging Reference Systems, Inc., USA
[2] NITS – National Institute of Standards and Technology, USA

Phantom of the human head was developed for MW stroke detection and classification in the article [25]. It is intended for the frequency range 0.5 GHz-3 GHz. It is anatomically and dielectrically realistic phantom mimicking five different anatomical parts – scalp, skull, cerebrospinal fluid, brain and stroke regions. Brain part is in liquid form to enable insertion of 2 different stroke models – ischemic and hemorrhagic. Other parts are made of different percentages of polyurethane rubber, graphite powder, acetone and carbon black powder. Concentric realistic phantom parts were 3D printed. MW system should be able to detect and classify stroke types according to the change of dielectric properties which would lead to faster treatment of a patient.

3D printable tissue-mimicking material is presented in [26]. The dielectric properties were evaluated over the frequency range 0.5-8.5 GHz. Solid phantom is based on ABS, SEBS and highly conductive carbon black. ABS is widely used for conventional 3D printing. Direct mixing of ABS with carbon black leads to fragile consistency, that is why SEBS is added. Broadband properties of phantom's variations do not mimic biological tissue very accurately; however, they do at discrete frequencies. Further investigation is necessary.

3.3 Gel Phantoms

It is advantageous for hyperthermia phantom to allow surface as well as interstitial applicators to be tested. For this reason, gel-based phantoms are the most suitable ones. The following part will be mostly focused on gel phantoms designed for hyperthermia and ablation. Materials developed to simulate the properties of biological tissue can be divided into several groups, according to the base ingredient [18, 27].

One of the first phantoms, designed by A.W.Guy in 1971, is based on a well-known gelling agent TX - 150 [1]. The composition of the phantom for simulating muscle consists of 76.5% saline solution (12 g salt per litre), 15.2% polyethylene powder and 8.4% TX - 150 (percentage by weight). Dielectric constant varies by the percentage of polyethylene powder. The salinity of material affects electrical conductivity. The article also describes phantom consisting of Laminac 4110 (a polyester resin), catalyst, acetylene black and aluminium powder for mimicking fat and bone tissue [28]. Cheung and Koopman modified both materials for X-band frequencies. The article studied properties of phantoms (muscle/fat and bone) over the frequency range 8.5 - 10 GHz [29]. It is suitable for mimicking muscle tissue, but it is difficult to achieve the standard gelation parameters [27–29].

The simplicity of preparation and low price are the benefits of the fat phantom based on flour developed in Utrecht (*The Utrecht Department of Radiotherapy and the Lund Department of Radiation Physics*). The phantom consists of flour, oil and saline solution (0.9% NaCl per litre) in weight ratio 500:225:25. Water content, as well as oil to some extent, controls dielectric constant. The problem is the low specific heat of the phantom [30].

Multispectral photoacoustic imaging is one example of the application where gel-wax based phantom with both acoustic and optical properties can be used as described in [31]. Scattering and optical absorption coefficients were adjusted by addition of TiO_2 and oil-based coloured inks.

[1] Oil Center Research Inc., USA, the refined product is TX-151

For testing, ablative thermal therapy devices (which use temperatures above 60°C) was developed another novel phantom made of thermochromatic ink and polyacrylamide that permanently changes colour from white to magenta according to the temperature [32]. The advantage of this phantom is the visualisation of ablation volume and geometry, as well as the peak of maximal temperature. Another thermochromatic type for high intensity focused ultrasound was introduced in [33]. The phantom is composed of thermochromatic ink, silicon dioxide and bovine serum albumin and can be used for characterization HIFU heating without MRI or thermocouples.

Polyacrylamide phantoms are suitable because of their gel structure, high melting point and optical transparency. The greatest limitation is a complicated fabrication process, the toxicity of some chemicals, and the durability spans weeks at most [18].

3.3.1 Gelatin Phantoms

Another alternative is a phantom based on gelatin and water. The article by Lazebnik et al. [27] describes a phantom based on oil-in-gelatin dispersions, different biological tissues are mimicked over the frequency range from 500 MHz to 20 GHz. The phantom is designed primarily for modelling breast tissue – fat, muscle, skin. The emphasis lies on time stability even when joining two kinds of samples with different oil proportion – when joined, there should be no diffusion. Relative permittivity and conductivity were monitored over eight weeks. Phantom with a lower proportion of oil (0-10%) simulates the electrical properties of the tissue with high water content – muscle. On the other hand, a phantom with a higher proportion of oil (70-80%) models low-water content tissue – bone, fat. It is also possible to model skin where the oil content is then 25%. The oil has a very low permittivity, the higher the quantity, the lower the permittivity. For muscle tissue modelling in the range from 915 MHz to 2.45 GHz, the phantom with 10% oil content is the most suitable one for ablation. Cancerous tissue can be approximated very well by 10% oil content (80% for fat tissue and 25% for skin tissue), it is intended primarily for microwave detection of breast cancer in the frequency range of 1 to 11 GHz [27].

Articles by Lazebnik et al. were expanded by Joachimowitcz et al. [34] in order to complement the research focused on breast cancer detection up to 6 GHz. The study proposes a mixture consisting of oil and gelatin, its drawback is shorter preservation time. The second possibility composing of TX-100, water and salt has longer time stability. The latter mixture is also advantageous for 3D printing. Binary fluid mixture model was prepared to predict the permittivity as a function of water and TX-100 percentage. Conductivity could be predicted from salinity. Breast and head phantoms fabricated from 3D printed structures and liquid mixtures are described in the article by the same research group in [35]. The goal of the study was the anthropomorphic model intended for pre-clinical application testing. Head and breast model was printed from ABS. Three cavities in the model were filled with different fluid TX-100-salted mixtures. ABS structure (representing the skull in head case) was a trade-off between wall stiffness, tightness and low field perturbation.

Analyses of various mixture solutions which can accurately mimic the dielectric properties of biological tissue are presented in the study by Pollacco et al. [36]. The focus was on muscle and adipose (fat) tissues over the frequency range 500 MHz to 50 GHz.

Different concentrations of BSA dissolved with PBS and Ringer's solution [1] were prepared to evaluate their influence on dielectric properties and compared to muscle dependence. Versions consisting of peanut oil and TX-100 in PBS and Ringer's solution were fabricated for mimicking adipose tissue. The effect of each substance on dielectric properties is described in the study. Specific concentrations were proposed for muscle and fat mimicking phantoms.

In an up-to-date article [38] was proposed breast tissue-mimicking phantom for testing novel millimetre-wave breast cancer detection system. The imaging system is based on the dielectric contrast between healthy and cancer tissue. The mixture is composed of sunflower oil, water, dishwashing liquid and gelatin. Dielectric properties were measured in 0.5-50 GHz frequency range by coaxial probe kit. The target frequency is 30 GHz. Alternative solidifying agent – waste-oil hardener was examined and proposed. Detailed fabrication and preservation (in oil) are explained. Composition of material mimicking various malignant tissues is presented consisting of different amount of solidifying agent. The study represents the first step to heterogeneous breast phantom.

Gelatin phantoms are used also for ultrasound applications. Required properties are obtained by the mixture of gelatin, alcohol, graphite powder and preservatives. Material based on this composition has long-time stability, but low thermal stability. Another example of the phantom for such application is gelatin mixed with alginate [20].

Long-time stability, low price, and easy preparation are the benefits of gelatin phantoms. The basis is gelatin mixed with water, by adding other substances is possible to achieve desired properties. Electrical properties can be tuned with an addition of honey syrup with ethylene diol and polyethylene powder as preservatives. The main limitations of the gelatin phantoms are their low mechanical strength and low melting point. Both thermal and mechanical properties can be improved by an addition of formaldehyde [18, 27].

3.3.2 Agar Phantoms

Agar is a gelatinous polysaccharide that is made from several types of seaweed, especially from red algae - Gelidium and Gracilaria. It is very resilient in cold water, and it can endure up to twenty times its weight. When an agar solution is heated above 85 °C and then cooled down to the room temperature, it solidifies into a body with a gelatinous consistency. The freezing point is 32-40 °C. Agar powder is widely used for preparing hyperthermia phantoms [39].

Agar phantoms have been widely used for mimicking human tissues at ultrasound frequencies because of its similar acoustic properties. Gel phantom with agar concentration lower than 4% has comparable porosity as soft tissue such as brain tissue. Higher agar concentrations can mimic microstructure of e.g. bones [40].

One of the first compositions of agar phantoms designed for hyperthermia comes from the Japanese scientists Kato and Ishida. The first phantom was designed to test RF hyperthermia at 13.56 MHz. It consists of three components – agar powder (2%), NaCl (0.43%) and water (97.57%). This phantom was simulating muscle tissue (specifically modelled on the femoral muscle of the cow). It is one of the first recipes, previously widely used.

[1] Ringer's solution – solution composes of sodium chloride, potassium chloride, calcium chloride, and sodium bicarbonate in such concentrations which correspond body fluids [37].

The disadvantage is a problem with preservation when it is stored for longer periods: a mould develops, and water separates from the phantom (that leads to the change of parameters) [41]. The recipe was later modified with an addition of azide as a preservative [42].

Another recipe for 5-40 MHz frequencies is as such: the principal ingredient is agar powder, additional substances are PVC (polyvinyl chloride) powder, sodium azide (NaN_3) and water. The concentration of agar powder in this composition is 4% in water, PVC powder ranges from 0 to 44.4%, and the sodium azide percentage is changed from 0 to $8 \cdot 10^{-3}$ %. Materials must be mixed and heated to obtain a gel form. Permittivity does not depend on the concentration of the azide; it decreases linearly with increasing concentration of PVC. The electrical conductivity increases linearly with azide in water and exponentially decreases with increasing concentration of PVC. Sodium azide serves as a preservative; the model lasts up to one-year [43].

Ito, Furuya, together with other scientists, created an agar phantom that represents the electrical parameters of a high-water content tissue suitable for the 300 MHz to 2450 MHz band. The phantom is made of agar powder, deionized water, TX-151, PE powder, NaCl and a preservative (sodium azide). Sodium azide is a highly toxic substance, but just a small amount of it is used in this study. The azide also influences electrical conductivity. No expensive device is needed to create a phantom. The polyethylene powder is used to modify relative permittivity, while the electrical conductivity is adjusted by the proportion of NaCl (but also PE) in particular. The agar solution cannot be mixed with PE powder directly, so the TX-151 is used to increase its viscosity. The amount of TX-151 is dependent on the amount of PE powder; the exact formula for the calculation is presented in ref.[44]. It has good mechanical properties and shelf life of at least one month when wrapped in plastic film with a preservative. In the article, there are suggested other preservatives as an alternative to sodium azide with an equivalent amount of NaCl [44].

Article [45] deals with high-water content phantoms for SAR measurement in the 3-6 GHz frequency band, the composition of the phantom is a variation to Ito recipe [44]. The electrical conductivity depends on the amount of PE powder and NaCl, whereas relative permittivity depends only on the PE powder content. The desired properties were achieved primarily by determining the amount of PE powder according to the required permittivity and then by calculating the amount of NaCl in the given ratio. The difference between the actual values and values reached by the phantom was ±5%.

Ultrasound testing also uses agar-based phantoms made of agar, water, propanol due to its well-characterized performance, availability, good thermal stability and ease of fabrication. Evaporated milk can be added for increasing attenuation. An alternative mixture consists of agar, water, glycerol, benzalkonium chloride, SiC powder and Al_2O_3 powder is described in [20]. Ultrasonic (and magnetic) hyperthermia can be enhanced by using sonosentizers [1] which increase the effectiveness of increasing the temperature, thus, the effectiveness of therapy. Scattering effect of nanoparticles was tested by their insertion in agar solution with homogeneous structure since the agar has convenient acoustic properties. Acoustic properties of such enhancement were then examined and evaluated in [40].

[1] Magnetite nanoparticles that attenuate ultrasonic waves and dissipate the energy to the tissue in the form of heat.

Thermostability of agarose-based tissue-mimicking material was studied in [46]. The goal was further investigation of the agarose gels properties since it is commonly used TMM. Spectral changes of the material were insignificant after heating it to 70 °C, irreversible changes appear around 80 °C. Time stability of agar TMM over 4 years is presented in [47]. Ultrasonic properties (thickness, speed of sound, attenuation coefficient) were investigated and compared to the reference values. Results show that the properties did not differ statistically from the standard reference.

Due to the high melting point (approx. 80 °C), agar phantoms are suitable for applications requiring higher temperatures (ablation, hyperthermia). They have sufficient mechanical properties to create a large sample. On the other hand, they are relatively fragile. Electrical properties can be adjusted by the proportion of individual phantom components.

In general, it is difficult to achieve the same relative permittivity as in biological tissue. Many other phantoms in other forms have been proposed to simulate the electrical properties of various biological tissue. Various types of phantoms are suitable for different applications [18].

3.4 Summary of Ingredient's Function

Functions of chosen commonly used components for phantom fabrication are summarised in Tab.3.1.

Table 3.1. Summary of ingredient's function, inspired by [48] and own observations.

Component	Function/role
Distilled water	Mainly increases complex relative permittivity, to fabricate high-water content TMM
Sodium chloride	Increases imaginary part of complex relative permittivity; and conductivity
Sugar	Decreases relative permittivity and slightly reduces conductivity
TX-100	Emulsifier; reduces complex relative permittivity
TX-150	Solidyfier; increases viscosity and homogeneity
TX-151	Solidyfier; increases stickiness; prevents thermal convection currents
Sodium azide	Preservative; increases conductivity in water solution
Graphite	Increases conductivity
Agar;Gelatine	Gelling agent; solidifier
Oil	Fabrication of low-water content TMM
Silicone	Carriers carbon; provides consistency; emulsion for controlling relative permittivity
Acrylamide	Lowers relative permittivity; slightly increases conductivity; strengthener
PVC	Decreases both permittivity and conductivity

Chapter 4
Measurement of Dielectric Properties

Dielectric measurements are quite complex, and there is no single technique capable of characterizing any material over an entire frequency range. This chapter is focused on measuring polar materials which have strong frequency dependence. Particularly polar liquids have two important applications - as a reference material which is used for calibration and as the components of tissue-mimicking materials. Factors which significantly influence the decision to use a particular method are [17, 49]:

- Frequency band
- Required accuracy
- Temperature range
- Material form
- Sample size/thickness
- Contact/Non-contact method
- Destructive/Non-destructive
- Price

The methods are mainly divided into these classes [17, 49]:

- Reflectometric methods – measurement of S-parameters
- Transmission methods – measurement of S-parameters
- Resonance methods – measurement of Q-factor and resonant frequency

Other widely used methods are *free space*, *time-domain* and *capacitance-cell* methods.

Wave propagation also depends on permittivity, permeability and conductivity of the material in which the wave propagates. Let's assume that there is a material under test (MUT) in free space and TEM wave incident on its surface. Because the wave has different impedance in the material than in free space, there is impedance mismatch which leads to the creation of reflected waves. Part of the energy also penetrates the sample. The impedance in the material is lower (relative to the free space), the wavelength is shorter, the velocity in the material is lower and the magnitude of wave in the sample is attenuated [10].

$$Z = \frac{Z_0}{\sqrt{\varepsilon'}} \tag{4.1}$$

$$Z_0 = \sqrt{\frac{\mu_0}{\varepsilon_0}} = 120\pi \tag{4.2}$$

$$\lambda_{material} = \frac{\lambda_0}{\sqrt{\varepsilon'}} \tag{4.3}$$

$$v = \frac{c}{\sqrt{\varepsilon'}} \tag{4.4}$$

For reflectometric and transmission methods of measurement, the reflection from and the transmission through a material is used to obtain required parameters. For this type of measurement, a vector network analyser or impedance analyser must be available. VNA consists of a signal source, a receiver and a display. Signal source launches a signal to the material which is examined (MUT) at a certain frequency. The receiver is tuned to the same frequency for detecting reflected and transmitted signals. Results are magnitude and phase at a particular frequency. Then the source is tuned to another frequency and the process repeats. To eliminate systematic measurement errors, device calibration must be performed. However, random errors such as noise, drift, temperature, humidity and pressure cannot be eliminated by the calibration. The correct measurement methodology is necessary for the smallest uncertainty. Different dielectric measurement techniques are discussed below [10].

4.1 Transmission Line Methods

Transmission line measurement has following advantages [10]:

- Broadband – low end is limited by the practical sample size
- Measuring magnetic materials
- Anisotropic material can be measured in a waveguide

During this measurement, the sample is placed inside the centre of an enclosed transmission line, which is the greatest disadvantage of this method. It is usually a section of rectangular waveguide or coaxial line. The MUT must satisfy certain criteria such as homogeneity and must fill the entire cross-section area of the line. Full attachment with no air gaps must be obtained. Dielectric parameters are obtained from the measurement of both reflected and transmitted signals, i. e. S - parameters S_{11} and S_{21} or S_{22} and S_{12} since complex relative permittivity can be calculated from each of the four S - parameters. More accurate results for higher frequencies could be obtained from transmission measurements; however, smaller uncertainty is computed from reflection measurements for radio frequencies. A two-port method is used for gel and solid materials. This technique is typically used up to 10 GHz. An advantage is easy thermal control as there is no thermally isolated inner conductor like in a coaxial probe. [10, 17, 49]

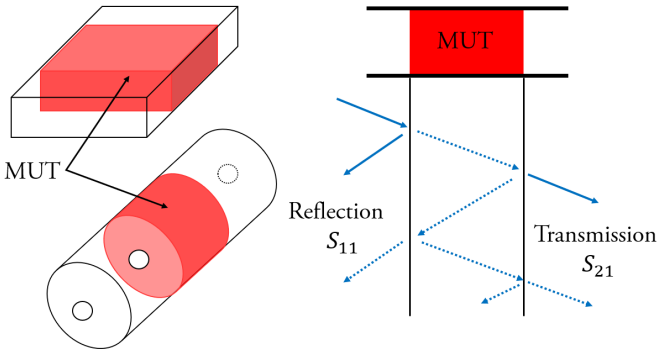

Figure 4.1. Transmission line measurement principle – waveguide, coaxial line. Simplified from [10].

4.2 Free Space Method

Advantages of this method are [10, 50]:

- No contact, non–destructive process
- High frequency (but sample size limitation)
- Suitable for high temperatures
- Magnetic materials measurement

Samples for measuring by this technique must be large, flat, parallel-faced and made from a homogeneous material. Reflection and transmission of EM waves depend on the contrast of their dielectric parameters. The equipment necessary to perform free space measurements consists of antennas focused at a sheet of the material under test, VNA and a fixture. The system is usually calibrated by through, reflect and line technique. Highly accurate calibration of the VNA may be difficult. Typically a thin sample is placed in front of the conductive plane and complex reflection coefficient is measured by VNA [10, 50].

$$\Gamma_1 = \frac{j \tan(k_0 t\sqrt{\varepsilon_r^*} - \sqrt{\varepsilon_r^*})}{j \tan(k_0 t\sqrt{\varepsilon_r^*} + \sqrt{\varepsilon_r^*})} \tag{4.5}$$

Where k_0 is the free-space number of electromagnetic wave and t is the thickness of the sample.

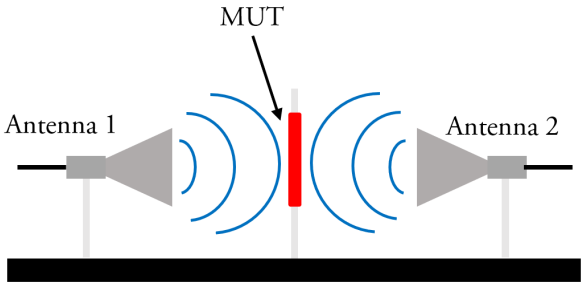

Figure 4.2. Free-space measurement principle. Simplified from [10].

4.3 Resonant Methods

The complex relative permittivity of typically homogeneous materials may be measured by using resonators and cavities. The main disadvantage of this technique is that it only measures at a specific frequency point; however its advantages are [10, 17, 49]:

- High impedance environment
- Possibility of small samples
- Well–suited for low loss materials
- High-temperature measurement range - from very low to very high temperatures

Resonant cavities are structures that resonate at particular discrete frequencies. The main principle is that the sample inserted into a cavity affects the resonant frequency and the quality factor (Q) of the cavity. Then the complex permittivity at a single frequency can be obtained. The measurement system consists of a VNA, a fixture and a resonant cavity. The system is designed in either TE mode or TM propagation mode.

The first step is to measure the resonant frequency f_1 and quality factor Q_1 of an empty cavity. Then repeat the measurement with the sample inside - f_2,Q_2 and compare. The dielectric parameter of the sample is computed as [10, 17, 49–50]:

$$\varepsilon_r = \left(\frac{f_1}{f_2}\right)^2 \tag{4.6}$$

$$\tan\delta = \frac{1}{Q_2} - \frac{1}{Q_1}\sqrt{\frac{f_1}{f_2}} \tag{4.7}$$

For smaller samples, the *perturbation technique* is used when sample is situated in the maximum of electric field inside the rectangular cavity operating in TE propagation mode. Complex relative permittivity is defined as:

$$\varepsilon_r = 1 + \frac{1}{2}\left(\frac{f_1 - f_2}{f_2}\right)\frac{V}{v} \tag{4.8}$$

Where V is the volume of the cavity and v is sample volume. Such method is shown in Fig. 4.3.

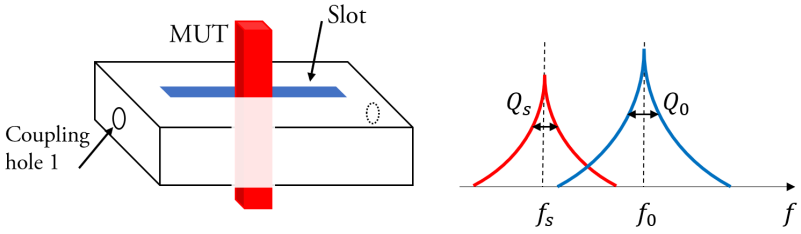

Figure 4.3. Resonant cavity measurement principle, cavity perturbation. Simplified from [10].

4.4 Parallel Plate (Electrode) Method

This technique is basically a thin sheet of material or liquid sandwiched between two electrodes which principally creates a capacitor. LCR meter or impedance analyzer can be used for the measurement. The capacitance and dissipation are measured in order to obtain the permittivity with the knowledge of dimensions of the MUT. The sample must be placed in such a way that there are no air gaps between the plate and material's surface. The method is explained in Fig. 4.4. This method is convenient for accurate, low frequency measurements (under 1 GHz) of thin solid samples and liquids. Complex permittivity is calculated as [10, 49]:

$$Y = G + j\omega C_p = j\omega C_0 \frac{C_p}{C_0} - j\frac{G}{\omega C_0} \tag{4.9}$$

Where C_0 is the capacitance of air and A is an electrode area.

$$\varepsilon_r^* = \frac{C_p}{C_0} - j\frac{G}{\omega C_0} \tag{4.10}$$

$$\varepsilon_r' = \frac{tC_p}{A\varepsilon_0} \tag{4.11}$$

$$\varepsilon_r'' = \frac{t}{\omega R_p A \varepsilon_0} \tag{4.12}$$

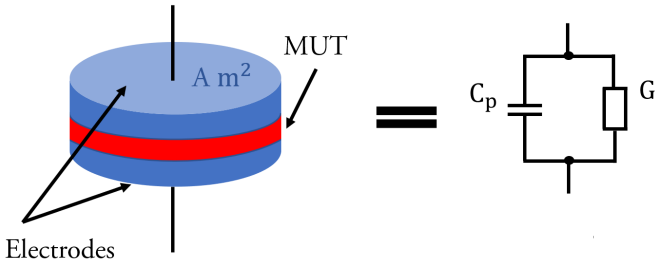

Figure 4.4. Parallel plate measurement principle and its equivalent circuit. Simplified from [10].

4.5 Inductance Measurement Method

This method is used for measuring effective permeability, which is obtained from the inductance measurement performed with an impedance analyser. The method is illustrated in Fig. 4.5. The relative permeability is calculated [10]:

$$\mu_r = \frac{L - L_s}{\mu_0} \frac{2\pi}{h \ln(\frac{c}{b})} \tag{4.13}$$

where h, c, b are height, inner diameter, outer diameter of MUT respectively, L is measured inductance with and L_s without MUT.

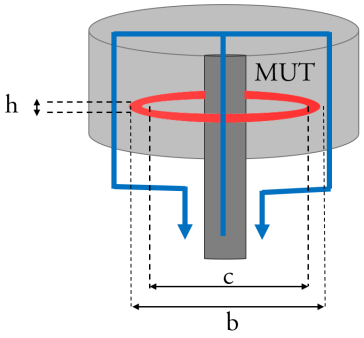

Figure 4.5. Inductance measurement principle. Simplified from [10].

4.6 Time-Domain Method

It is based on the measurement of time-varying signal responses from the sample when is excited by transient signal. MUT is usually placed at the end of the transmission line. The dielectric properties are obtained by converting time-domain information to frequency domain by using the Fourier transform. The method becomes less accurate for higher frequencies [17].

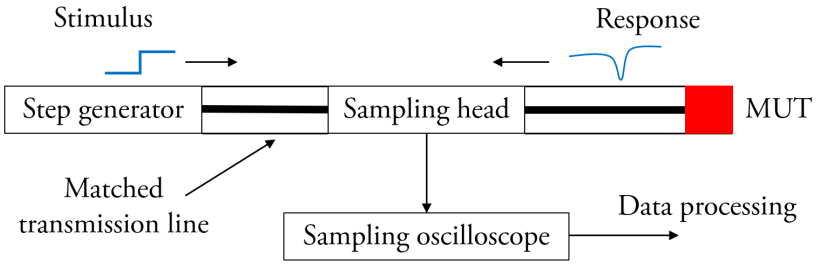

Figure 4.6. Time-domain reflectometry measurement principle. Simplified from [17].

4.7 Reflectometric Methods

There are many types of reflectrometric methods; one of the simplest is using short-circuited waveguide. However, the most common and convenient technique is coaxial sensor, also referred as coaxial probe and open-ended coaxial line. Coaxial probe measurements have many advantages such as [10, 17]:

- Broadband measurement range
- Simple and non-destructive procedure
- Best for liquids and semi-solids

The method is limited to non-magnetic, isotropic, homogeneous materials. The sample must also have a semi-infinite thickness according to the frequency band, and its surface must be flat. An open-ended coaxial probe is basically a cut section of a transmission line. The probe is inserted into the material or placed on the surface of the sample. The EM field at the probe's end penetrates the material and changes its properties (demonstrated in Fig. 4.7). The reflected wave (S_{11}) is then measured and analyzed to obtain the complex permittivity. Dielectric properties are then computed from its phase and magnitude [10].

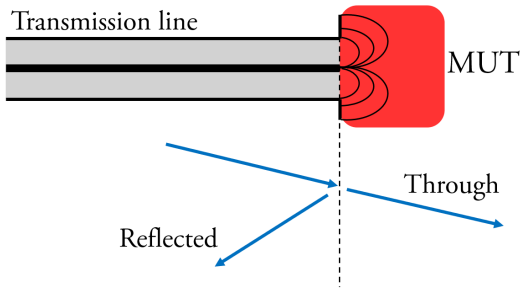

Figure 4.7. Open-ended coaxial probe measurement principle. Simplified from [10].

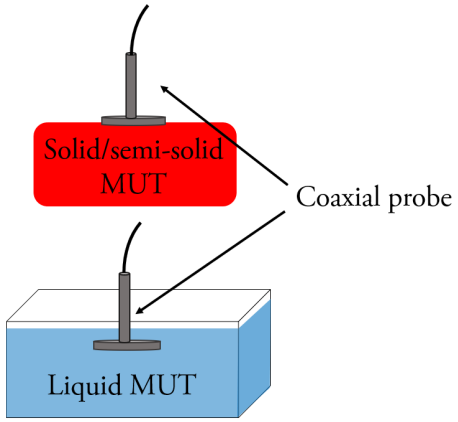

Figure 4.8. Different form of samples measured by the coaxial probe. Simplified from [49].

There are several types of coaxial probes on the market, for example, high-temperature probe [1] (no temperature dependence of the probe), slim form of the probe [2] , and performance probe [3] . The manufacturers also provide a special shorting for calibrating the device with the probe.

The most common way of calibrating the device is by using the single reference liquid method. The biggest problem is usually insufficient contact during short-circuit measurement; which more probable for small coaxial probes. The least-squares approach is applied to multiple measurements to lower this inaccuracy. Methanol (RF and MW), ethanol, acetone (up to 60 GHz) as well as pure water are liquids which are used as reference. Any reference liquid must have a well-know and accurately measured dielectric properties. Its convenient to use a reference liquid with similar complex permittivity in order to reduce the measurement's uncertainty. The main sources of errors of this technique are cable instability, air gaps and insufficient sample thickness [17].

It is convenient to test hyperthermia applicators (which can also be interstitial or intracavitary) on a gel form phantom. For this type of material, the best-suited is the coaxial probe. It enables quite simple and fast surface measurement of possibly even heated phantom, therefore coaxial probe measurement will be discussed in more details below.

The procedure of coaxial open-ended probe measurement for obtaining complex permittivity is as follows [51]:

- Calibration of one VNA port – open-short-load calibration at the end of the measuring cable
- Connecting the probe
- Measuring S_{11} of a standard – a liquid with well-known dielectric properties at a specific temperature
- Conversion of S_{11} to Y, equation (4.14)
- Obtaining G_0 and C_0 by finding solution of equation (4.16), where ε is known
- Measuring S_{11} of MUT and obtaining ε by finding solution of equation (4.16), where G_0 and C_0 are known

$$S_{11} = \frac{Y_0 - Y_{meas}}{Y_0 + Y_{meas}} \tag{4.14}$$

$$Y_0 = \frac{1}{Z_0} \tag{4.15}$$

$$Y = j\omega\varepsilon C_0 + \sqrt{\varepsilon^5} G_0 \tag{4.16}$$

[1] Keysight Technologies, Inc., USA
[2] Keysight Technologies, Inc., USA
[3] Keysight Technologies, Inc., USA

Chapter 5
Design of Tissue-Mimicking Phantom

The electrical conductivity and complex permittivity (real and complex part) are the primary dielectric properties for microwave applications. The agar type of phantom was selected for our phantom design due to its easy preparation, availability and high melting point. Gel form has been selected because of its versatility for testing hyperthermia applicators. The composition by Ito [44] has been chosen from detailed examination because it is suitable for simulating muscle tissue, is intended for a frequency range of 434-2450 MHz and the article contains the fabrication procedure.

A basic mixture was prepared according to Kato [41], which consists of water, agar powder and sodium chloride and is designed for frequency of 13.56 MHz.

Table 5.1. Composition of muscle equivalent phantom from the reference by Kato et al. [41].

Ingredients	Weight (%)
Water	97.50
Agar powder	2.00
Solidum chloride	0.43

The phantom was twice prepared according to ref.[44] following the proposed procedure, but the same results as in the ref.[44] were not achieved with the available equipment and without sodium azide. The composition of this phantom shows Tab.5.2. According to the procedure, the TX-151 was not possible to mix uniformly with the final mixture. Therefore, a different phantom preparation process was used. Deionized water, agar powder, TX-151, and sodium chloride were brought to a temperature above 85 °C, the heater was switched off, and the PE powder was then admixed. With this procedure, all ingredients were mixed sufficiently to form a homogeneous mixture. However, the prepared sample did not reach required values of the relative part of the complex permittivity and electrical conductivity listed in the ref. [44]. The measured values are shown in Figs. 5.1, 5.2. The reference values of muscle tissue are plotted from ref. [19], legend Muscle.

Table 5.2. Composition of muscle equivalent phantom reference by Ito et al. [44].

Ingredients	Weigh (g)
Deionized water	3375.0
Polyethylene powder	337.5
TX-151	84.4
Agar powder	104.6
Sodium chloride	37.6
Sodium azide	2.0

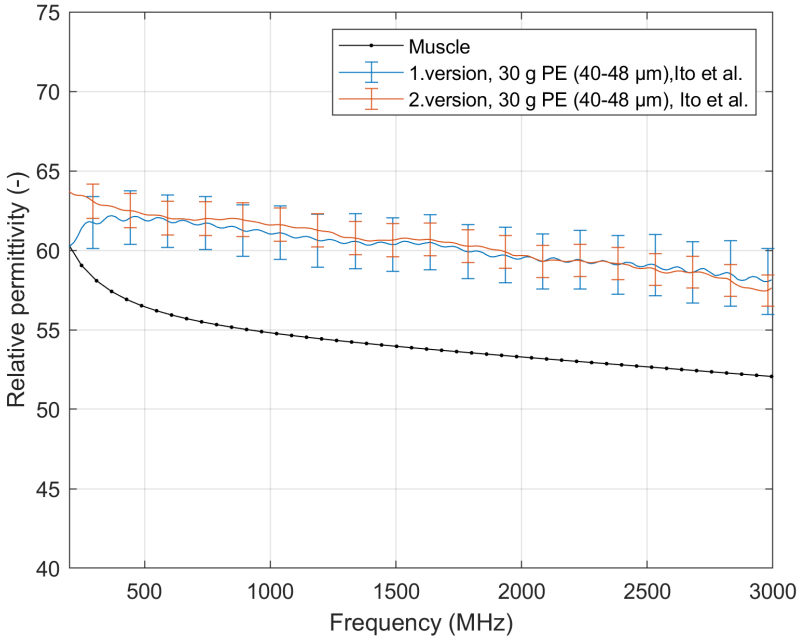

Figure 5.1. Relative permittivity with errorbars of samples prepared by the ref.[44] along with the muscle tissue properties by IT'IS Foundation [19].

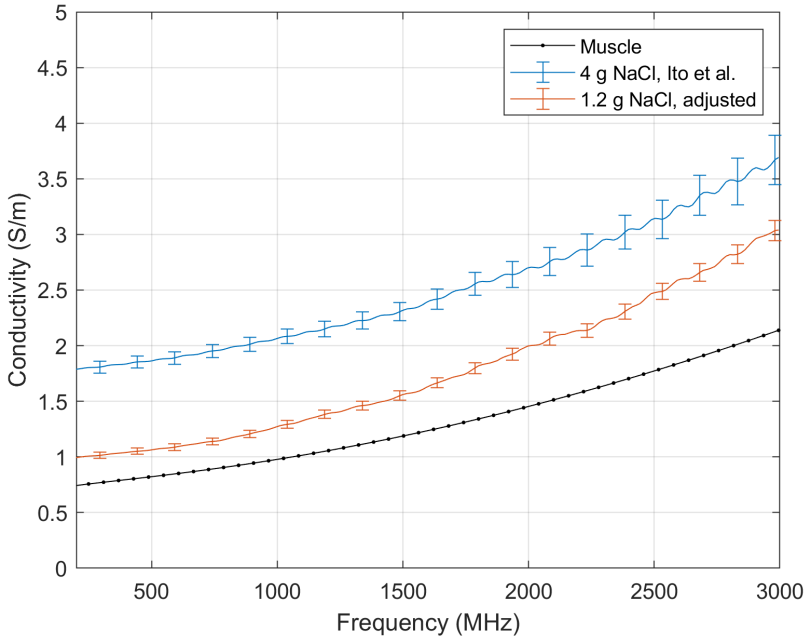

Figure 5.2. Conductivity along with errorbars of samples prepared by the ref.[44] along with the muscle tissue properties by IT'IS Foundation ref.[19].

Thus, it was crucial to modify the phantom composition to obtain the required properties. Overall more than 25 different versions were prepared, only the best ones are presented in this work. Preparation and measurements were performed at the Faculty of Biomedical Engineering, CTU in Kladno. The relative permittivity is adjusted by the proportion of PE powder and water; the electrical conductivity is adjusted mainly by the amount of sodium chloride, less so by PE powder. No preservative which could influence one or the other variable was used.

Various composition variations were prepared, based on a change of the proportion of PE powder and sodium chloride in the resulting mass to get lower permittivity and conductivity. It was necessary to increase the proportion of PE powder in the mixture to reduce permittivity. Sodium chloride concentration was decreased in order to reduce the conductivity. Deionized water in amount of 300 grams was always used while changing proportions of other substances. Figures 5.3 and 5.4 below show the results of different versions with various proportion of PE powder and sodium chloride.

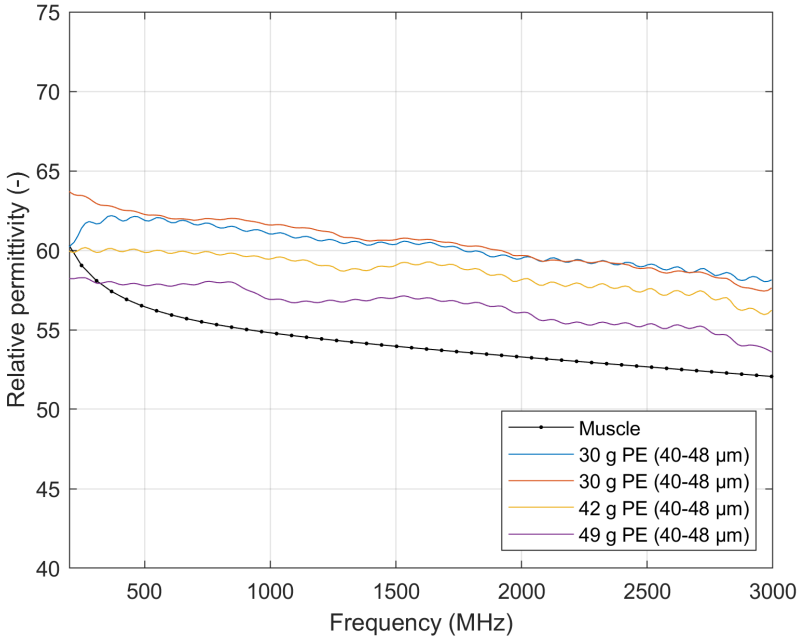

Figure 5.3. Relative permittivity of samples with varying proportion of PE powder along with the muscle tissue properties by IT'IS Foundation [19].

By increasing the proportion of the PE powder the permittivity decreases. Conductivity is significantly affected by the presence of sodium chloride, less so by the proportion of PE powder. By decreasing NaCl, the conductivity decreases. Both mechanisms are demonstrated in Figs. 5.3,5.4. The best result was achieved with a phantom of 49 g of PE powder per 300 g of water. Many air bubbles might have gotten into the sample during the preparation which might have affected the measured results; thus, our phantom fabrication process requires a vacuum system for the elimination of air bubbles. The amount of TX-151 is dependent on the amount of PE powder (the exact relation is shown in ref. [44]), so the amount of TX-151 has to be changed when changing the proportion of PE powder. Therefore the consistency of the final mixture also changes. The mixture with 49 g of PE powder was relatively solid, so the use of a vacuum system to remove bubbles was more difficult than with 30 g of PE powder in the mixture.

Variations of the agar phantom with honey or grape sugar have also been investigated; both materials are inexpensive, safe and easily accessible. Honey and sugar affect phantom's relative permittivity; electrical conductivity is determined by the proportion of sodium chloride in distilled water. The possible substitution of PE powder with the cheaper material – grape sugar has been inspected.

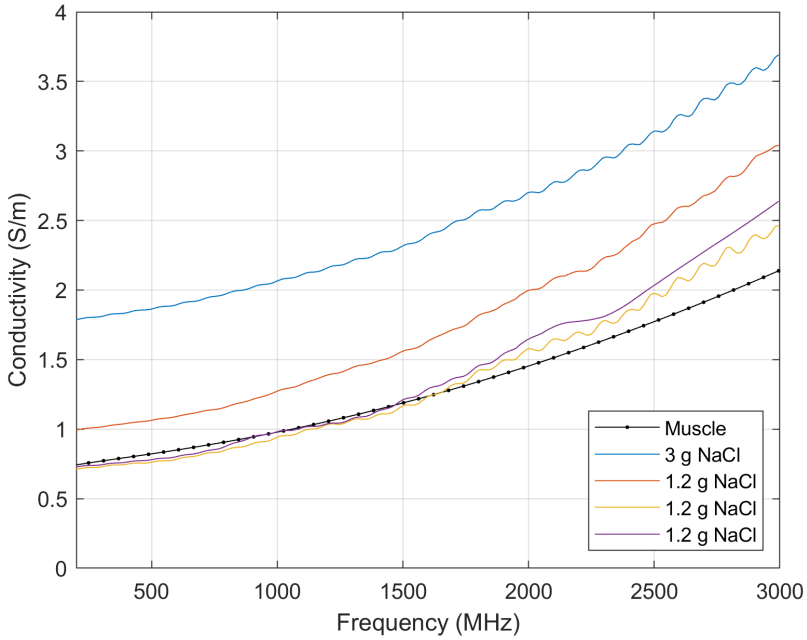

Figure 5.4. Conductivity of samples with varying proportion of sodium chloride and PE powder along with the muscle tissue properties by IT'IS Foundation [19].

However, measured data shows that fully replacing PE powder is not feasible. With an increase of sugar or honey, it is also necessary to increase the amount of agar powder or TX-151 in order to get solid consistency. For all sugar/honey versions, the preparation process was as following: the agar powder was mixed in distilled water with NaCl, then sugar/honey (optionally, TX-151 powder was added). The mixture was brought to 85 °C; then a vacuum system was used. The mixture was cooled down to room temperature and then covered. When a mixture is too dense, it is impossible to use the vacuum system, and the air bubbles remain in the mixture (an example is 34% sugar sample with TX-151). Figures 5.5 and 5.6 show measured values of the samples with various percentage of honey. With an increasing presence of honey, there was a problem with the stiffness of the phantom. Figures 5.7 and 5.8 show samples with various percentage of grape sugar, which proved to be better for the preparation of a phantom than with the honey.

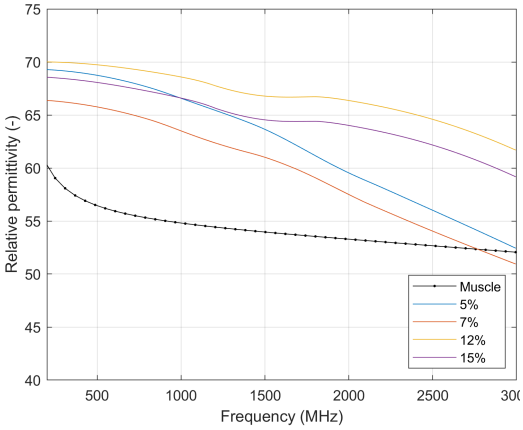

Figure 5.5. Relative permittivity with varying proportion of honey along with the muscle tissue properties by IT'IS Foundation [19].

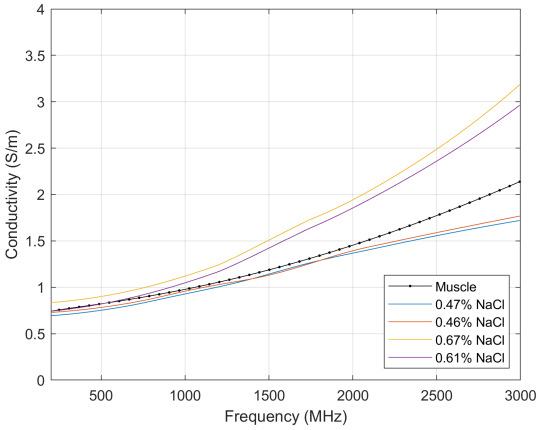

Figure 5.6. Conductivity of samples with varying proportion of sodium chloride along with the muscle tissue properties by IT'IS Foundation [19].

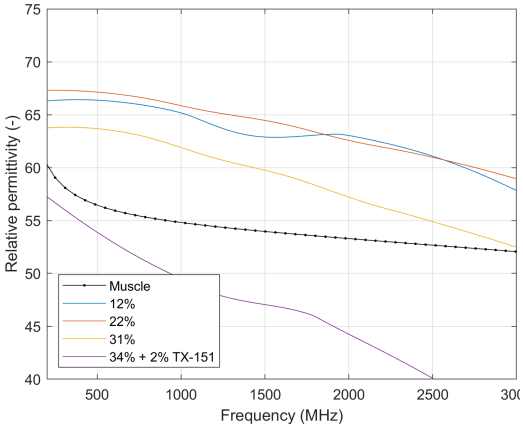

Figure 5.7. Relative permittivity with varying proportion of grape sugar along with the muscle tissue properties by IT'IS Foundation [19].

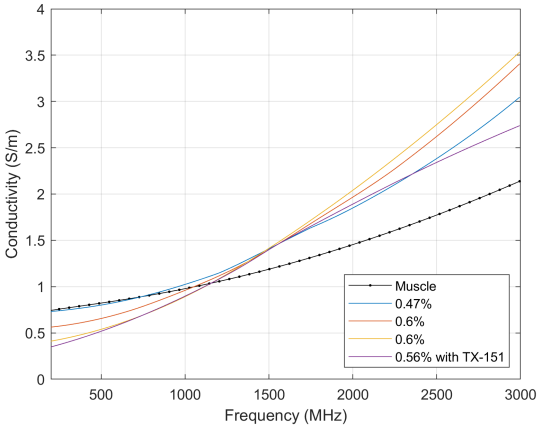

Figure 5.8. Conductivity of samples with varying proportion of sodium chloride along with the muscle tissue properties by IT'IS Foundation [19].

The best results, compared to Gabriel et al. [15], were achieved with the phantom that had a 13.23% concentration of the polyethylene powder. The detailed composition of the phantom is in Tab.5.3. Comparison of this phantom with muscle tissue is shown in the following Figs.5.9, 5.9 along with the uncertainty measure. This phantom was presented in the conference contribution [5]. Multiple measurements were performed to obtain measurement uncertainty. Figures 5.11, 5.12 compare the relative permittivity and conductivity between the measured values of the phantom prepared by Kato et al.[41], Ito et al.[44] and the proposed phantom. Long-term stability of the parameters was examined as displayed in 5.13, 5.14. The parameters did not change drastically during the week, even without any preservative.

Table 5.3. Composition of the proposed muscle equivalent phantom.

Ingredients	Weigh (g)
Distilled water	300.0
Polyethylene powder	49.0
TX-151	11.0
Agar powder	9.2
Sodium chloride	1.2

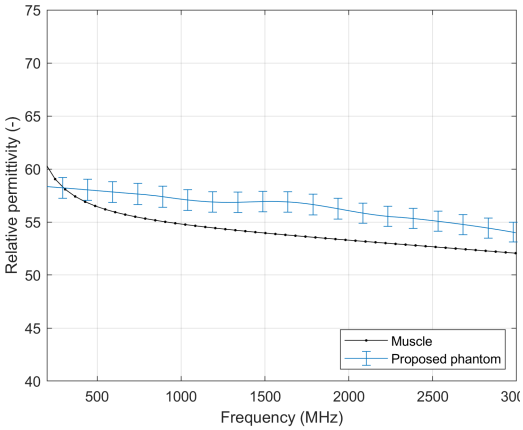

Figure 5.9. Relative permittivity of proposed muscle equivalent phantom along with the muscle tissue properties by IT'IS Foundation [19].

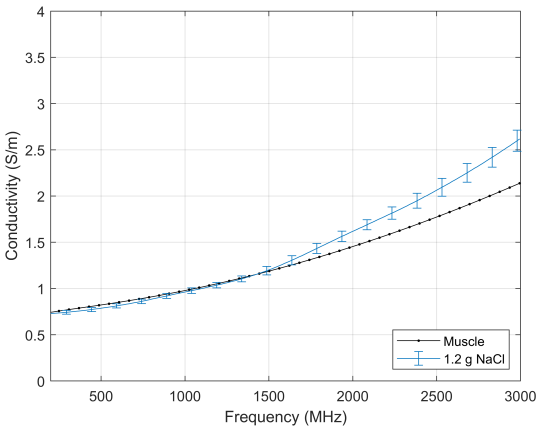

Figure 5.10. Conductivity of proposed muscle equivalent phantom along with the muscle tissue properties by IT'IS Foundation [19].

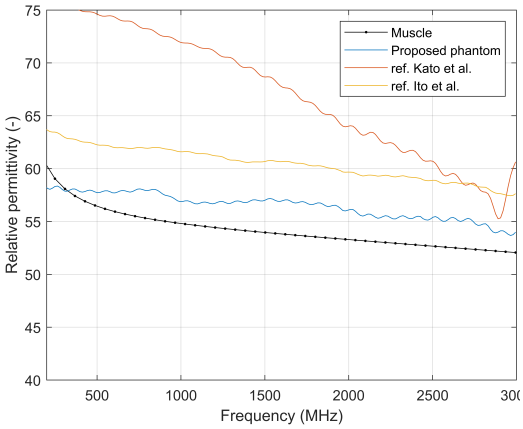

Figure 5.11. Comparison of measured values of the relative permittivity of Kato et al.[41], Ito et al. [44] and proposed phantom along with the muscle tissue properties by IT'IS Foundation [19].

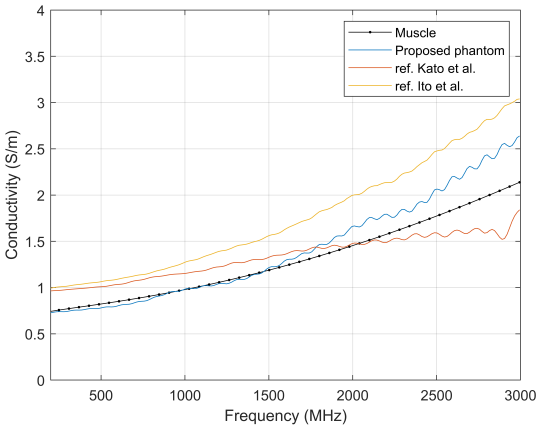

Figure 5.12. Comparison of measured values of conductivity of Kato et al. [41], Ito et al. [44] and proposed phantom along with the muscle tissue properties by IT'IS Foundation [19].

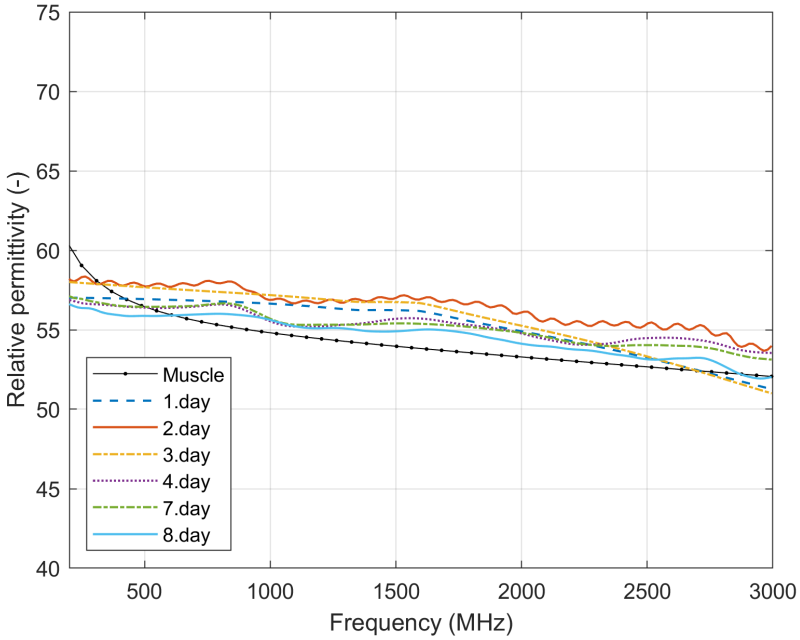

Figure 5.13. Relative permittivity of proposed muscle equivalent phantom measured one week along with the muscle tissue properties by IT'IS Foundation [19].

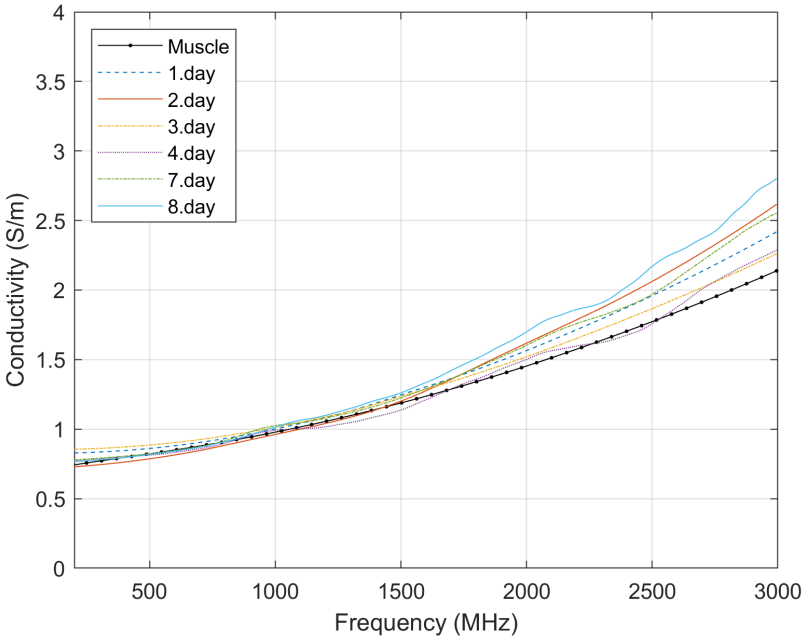

Figure 5.14. Conductivity of proposed muscle equivalent phantom measured one week along with the muscle tissue properties by IT'IS Foundation [19].

An article by Ley et al. [16] with the most recent research about the thermal dependence of dielectric properties of various biological tissues was published during the work on this thesis (further details in sec. 6). Since the phantom is also intended for testing non-invasive temperature measurement via UWB radar, the phantom has to imitate the temperature properties of a muscle. For this reason, temperature dependence of dielectric constant was tested at a temperature range of 25 °C to 50 °C. The procedure of such measurement is described in detail in sec. 6. The testing of the temperature measurement system brings new requirements on phantom properties, especially mechanical, therefore the phantom has to withstand temperatures around 50 °C. The temperature dependence of the T-M material earlier proposed in [5] does not correspond to the dependence of the muscle tissue as demonstrated in Figs. 5.15,5.16 so its composition was altered. Muscle tissue is identified as high-water content tissue, the water content in the phantom was increased to imitate its temperature behaviour. The proportion of distilled water along with proportion of PE powder was mainly adjusted in order to achieve the same properties. No preservative was used since it is not possible to use the phantom after warming it up. The composition of phantom was gradually changed. Version 1 and 2 differ in the volume of distilled water. Version 3 and 4 contain less PE powder and higher percentage of distilled water. Version 4 consists of 84% of distilled water and also 3.2% of TX-151 which ensures good mixing of the agar solution and PE powder as well as phantom's mechanical properties. The percentage of substances is summarised in Tab. 5.4.

Measurements of version 2 and version 3 are shown in appendix B.1. Version 1 has about 7.3 lower relative permittivity compared to the reference at 1.5 GHz, and at 25 °C; conductivity is 0.8 S/m lower. The phantom's permittivity of version 4 is 1.3 higher, and the conductivity is 0.3 lower. The relative permittivity descreases with temperature (and frequency). This behaviour occurs below *intersection point* after which the dependency reverses. This point is for the muscle at 6.5 GHz (acc.[16]), which is out of the observed frequency range of this work. Electrical conductivity of version 4 has cross-over point at 2.41 GHz, whereas, the muscle's intersection point is at 3 GHz [16]. Cross-over point of version 1 is at 2.3 GHz. The phantom frequency dependency mimicking ability is decreasing after this point, and it exhibits a higher absolute difference compared to the muscle tissue. The intersection point moves to higher frequency with each phantom version which is visible in presented figures. Version 2 also had worse mechanical properties; the phantom was very solid and tended to fall apart when heated.

Table 5.4. Composition of 4 consequent versions of the temperature-dependent phantom.

Phantom version	Version 1	Version 2	Version 3	Version 4
Distilled water (%)	81.00	81.50	82.75	83.88
Polyethylene powder (%)	13.23	12.80	11.08	10.02
TX-151 (%)	2.97	2.89	2.98	3.25
Agar powder (%)	2.48	2.49	2.53	2.30
Sodium chloride (%)	0.32	0.32	0.66	0.55

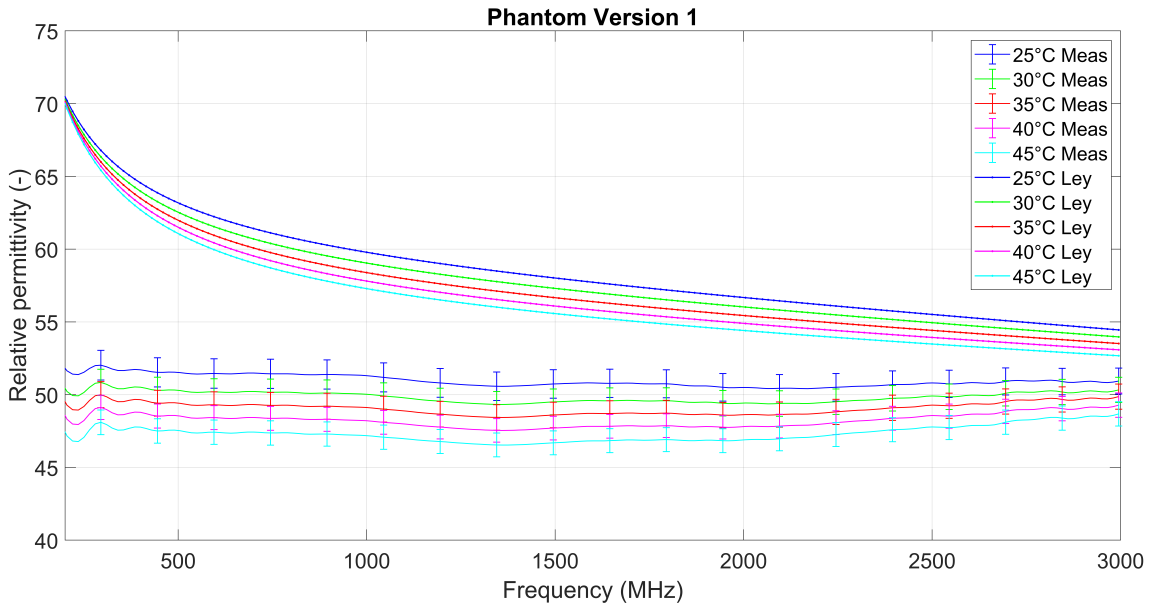

Figure 5.15. Relative permittivity's temperature dependence of phantom version 1 along with temperature dependence of muscle tissue according to Ley et al. [16].

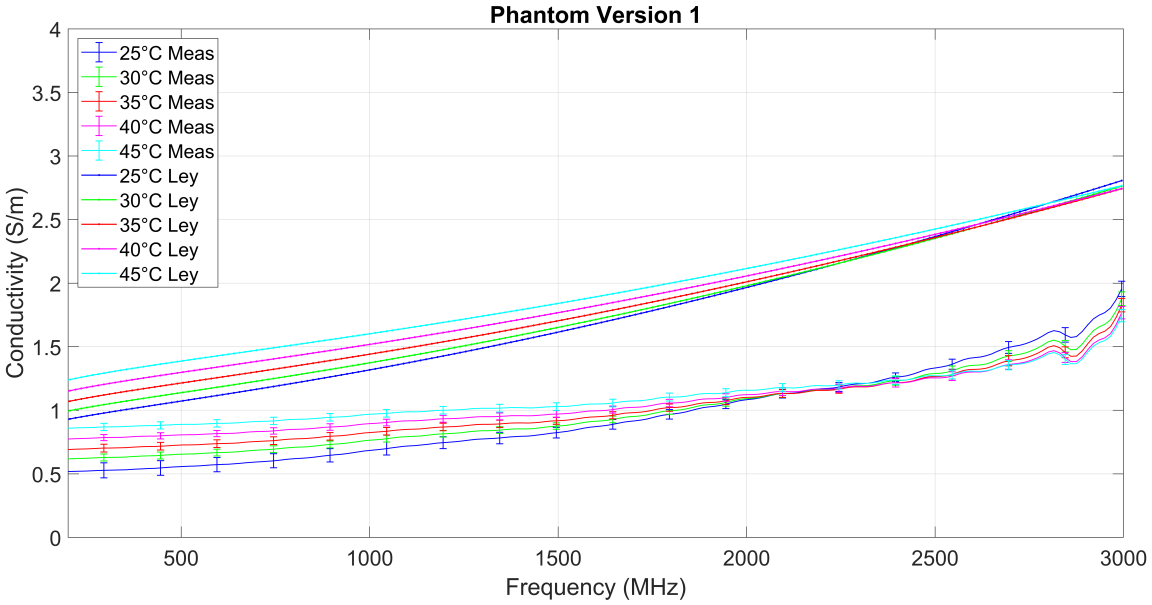

Figure 5.16. Temperature dependence of conductivity of phantom version 1 along with temperature dependence of muscle tissue according to Ley et al. [16].

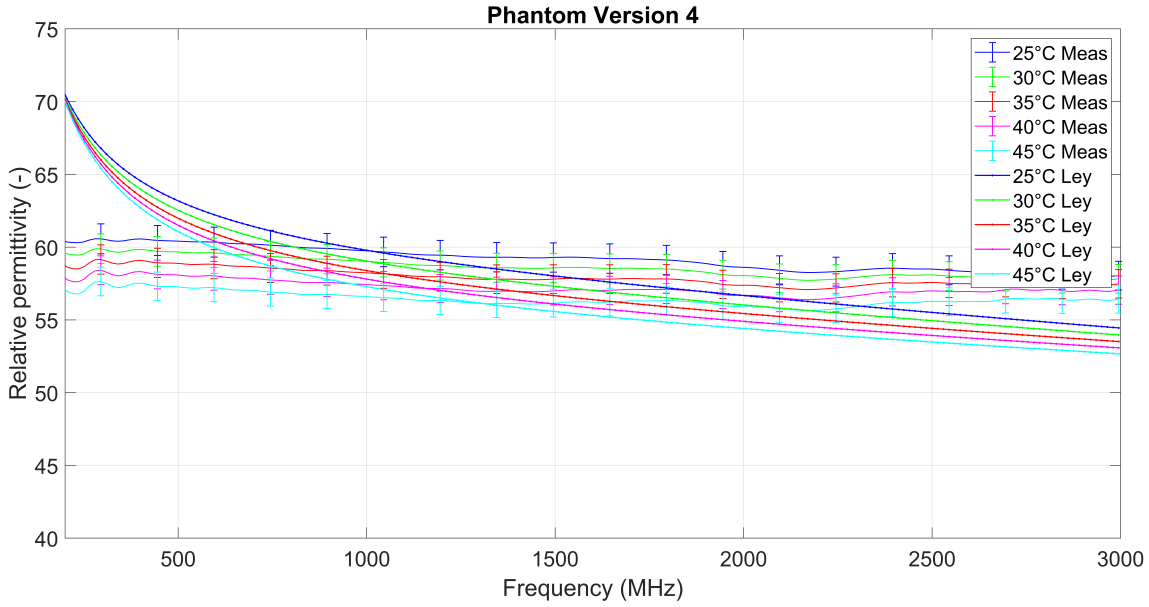

Figure 5.17. Relative permittivity's temperature dependence of phantom version 4 along with temperature dependence of muscle tissue according to Ley et al. [16].

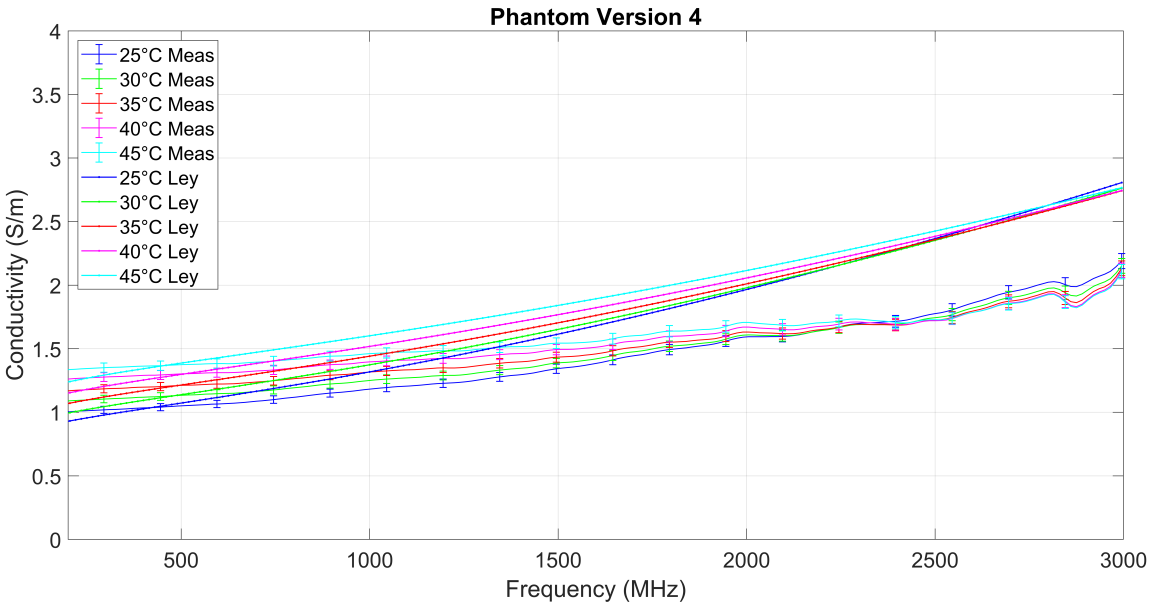

Figure 5.18. Temperature dependence of conductivity of phantom version 4 along with temperature dependence of muscle tissue according to Ley et al. [16].

Change in relative permittivity and electrical conductivity with the temperature is very important parameter when evaluating temperature dependence. The difference of these two quantities between each temperature step (a 5 °C step was chosen in this case) was observed at particular frequencies ($f = 1000, 1495, 2005, 2500$ MHz). Differences $\Delta\varepsilon_r'$, $\Delta\sigma$ were calculated to evaluate phantom's temperature behaviour. The results were compared with Ley et al. Absolute difference of relative permittivity between two temperature steps could be expressed:

$$\Delta\varepsilon_r'(f, \Delta\delta) = abs(\varepsilon'(f, \delta + 5°C) - \varepsilon'(f, \delta)) \tag{5.1}$$

Absolute difference of phantom's conductivity between two temperature steps:

$$\Delta\sigma(f, \Delta\delta) = abs(\sigma(f, \delta + 5°C) - \sigma(f, \delta)) \tag{5.2}$$

Where f are particular frequencies from which the differences were averaged. Parameter's changes are shown in bar charts 5.19, 5.20 for the phantom and the muscle tissue. The reference differences are blue bars. Ideally, phantom's bar should have the same height as the reference at the particular temperature step. Version 4 results have the smallest deviation compared to reference [16] at most of the temperature steps for both dielectric properties. Version 1 has overall the highest absolute difference in permittivity with temperature step.

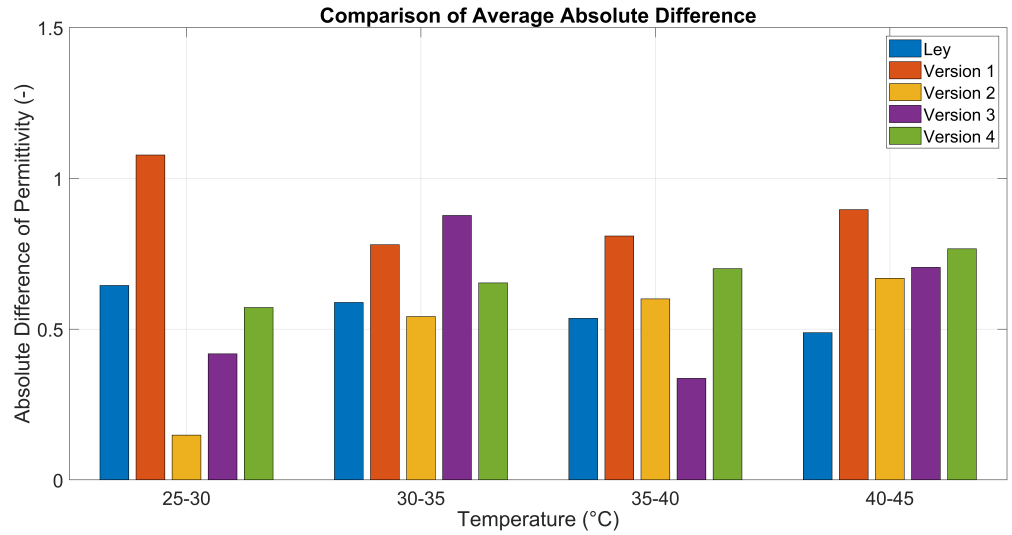

Figure 5.19. Comparison of average absolute difference in relative permittivity of phantom's different versions along with muscle tissue, according to Ley et al. [16].

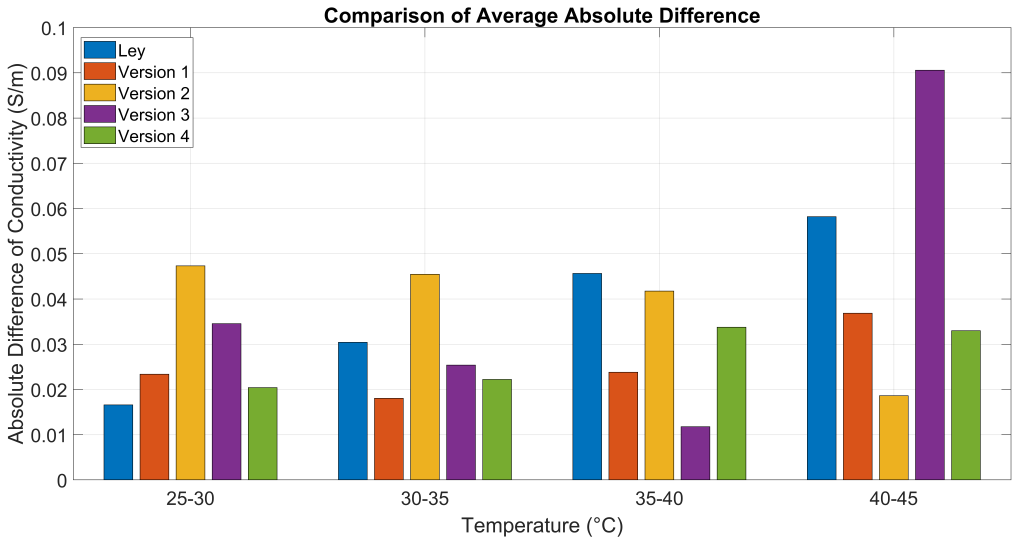

Figure 5.20. Comparison of average absolute difference in conductivity of phantom's different versions along with muscle tissue, according to Ley et al. [16].

Chapter 6
Tissue-Mimicking Phantoms Measurement

For this work, the relative permittivity and electrical conductivity of all phantoms were measured by using the open-ended probe kit SPEAG DAK - 12 in conjunction with handheld VNA Keysight FieldFox N9923A over the frequency range 10-3000 MHz. The measurement was performed at room temperature (approx. 22 °C) if not noted differently. The coaxial probe was attached to the sample after the calibration of the measuring system. A three-term calibration was performed by using Short-Open-Load at the port of VNA. Probe calibration evaluation the responses of probe when short circuited, in the air (open) and immersed 0.1M saline solution (load) at room temperature was carried out. As the short was used copper strip intended for higher frequencies, due to that is the measurement accurate at high frequencies and inaccurate at low frequencies, therefore only results in frequency range of 200 MHz to 3 GHz were evaluated. Measured reflection coefficient was processed in the PC containing the software for the calculations of dielectric parameters developed by SPEAG.

Precise measurement of the permittivity and conductivity are a great challenge because the accuracy of the calibration is affected by several conditions – the pressure of the probe to the sample, cable movement, temperature of individual parts – specially on the sample – and coaxial probes. Adhesion of the entire surface of the probe to the sample proved to be the most challenging part of the whole measurement, air gaps are very undesirable on the interface. However, excessive pressure on the sample should be avoided as well. A small water layer may be pushed out from the sample under too much pressure, which then leads to the measurement distortion. The basic measurement setup is shown in Fig. 6.1.

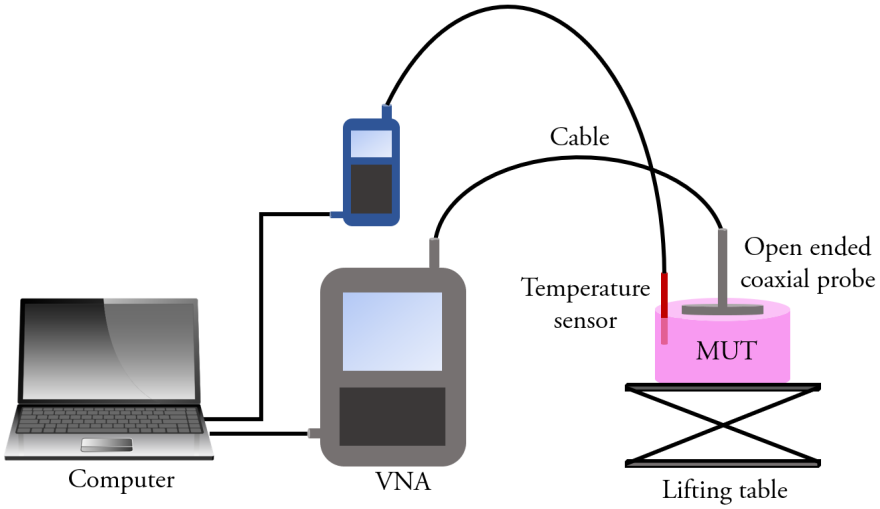

Figure 6.1. Basic measurement setup at room temperature.

Since the phantoms are also intended for testing the hyperthermia system in conjunction with UWB radar used for temperature measurement, it is necessary to test temperature dependency of dielectric parameters. Not many studies were published about this topic since the measurement is quite complex and time-demanding. Temperature dependence of livers (generally represents high water-content tissue) was studied for example in ref. [52]. In the study, liver tissue was placed in a laboratory oven and dielectric parameters were observed during heating and cooling phase. Another example of temperature-dependent dielectric spectroscopy was made by Ley at al. [16]. The study dealt with various porcine tissues (blood, liver, muscle, fat) and measured relative permittivity and conductivity in the temperature range from 30 °C to 50 °C. The data were modelled to a two-pole temperature-dependent Cole-Cole model which can be used in the frequency range 0.5 GHz to 7 GHz. The tissues were not heated in the oven like in previous study but in the hot water bath and by using hot plate and magnetic stirrer in case of blood.

As far as the author knows there is no recommended particular process of temperature measurement of the biological tissues or phantoms. New measurement approach of temperature-dependent dielectric parameters was proposed and verified in the contribution [6] by our research group. The aim was to reach higher accuracy and to suppress the uncertainties. The approach was based on the assumption from ref.[53] that temperature calibration reduces the inaccuracy. The difference between the Ellison reference for distilled water and the measurement was smaller for this temperature-dependent calibration as is illustrated in ref. [6].

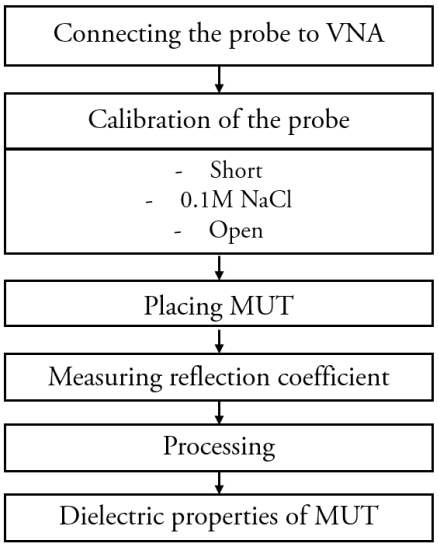

Figure 6.2. Flow chart of basic dielectric measurement.

Two identical phantoms were prepared before the measurement. Temperature calibration was performed ahead for all intended temperatures. The measurement setup is shown in the Fig. 6.3. Phantoms were placed in the heater's container with water. Two temperature probes were inserted into one MUT. One probe was situated in the middle and the other one close to the edge for observing homogenity of phantom's warming. The probe was positioned in such a way, so the complete contact with the surface of measured phantom was secured. It was possible to ensure certain temperature of the water in the container due to the heater. The phantom was considered uniformly warmed when the difference between the temperatures from center and edge probes was less than 0.2 °C. The heater was turned off.

Calibration data for that specific temperature were loaded, and the measurement was performed 10 times for each temperature and frequency. To warm up the phantom uniformly by 5 °C takes approx. 1 hour.

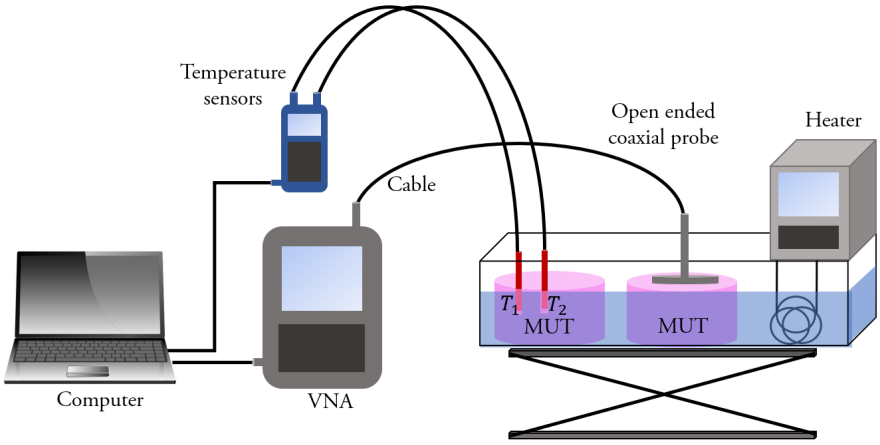

Figure 6.3. Measurement setup of temperature dependence of dielectric properties.

Figure 6.4. Actual measurement setup of temperature dependence of dielectric properties.

Chapter 7
Measurement Evaluation

Phantom of version no 4 was successfully tested and, based on the comparison with reference, approved for temperature-dependent applications. Frequency and temperature-dependent Cole-Cole model of measured data was determined. Such model is convenient because it enables to simplify the calculation of complex relative permittivity and electrical conductivity within the frequency and temperature measurement range. The same procedure was used in [16]. To model the dispersion accurately was used two-pole model. The whole computation was performed using MATLAB by Ley and the team [16].

$$\varepsilon^*_{r,fit}(\omega,\delta) = \varepsilon'_{r\infty,fit}(\delta) + \frac{\Delta\varepsilon_{1,fit}(\delta)}{(1+j\omega\tau_{e,1,fit}(\delta))^{(1-\alpha_{1,fit})}} + \frac{\Delta\varepsilon_{2,fit}(\delta)}{(1+j\omega\tau_{e,2,fit}(\delta))^{(1-\alpha_{2,fit})}} + \frac{\sigma_{fit}(\delta)}{j\omega\varepsilon_0} \tag{7.1}$$

Levenberg-Marquardt algorithm was used for data fitting to generally N-pole Cole-Cole model at each temperature. Two-pole model was estimated in this work. Values(s) α are usually fixed in the available references, α was fixed to value 0.1 for measured data in this case. The initial values were set according to Gabriel's parameters for muscle tissue and then adjusted. The parameters were computed by minimizing the mean absolute error. Parameters $\varepsilon_{r\infty,fit^*}$,$\varepsilon_{1,fit^*}$, ε_{2,fit^*}, τ_{1,fit^*} and τ_{1,fit^*}were estimated to fit the real part of complex relative permittivity. Then σ_{s,fit^*} was computed to fit imaginary part. Cole-Cole parameters denoted by * symbol were then used to determine the temperature dependence. Second-order polynomial with coefficients A_n,B_n, C_n was estimated to get the temperature dependence. For two-pole Cole-Cole equation are then the parameters defined as [52]:

$$\varepsilon'_{r\infty,fit}(\delta) = A_1\delta^2 + B_1\delta + C_1 \tag{7.2}$$

$$\Delta\varepsilon_{1,fit}(\delta) = A_2\delta^2 + B_2\delta + C_2 \tag{7.3}$$

$$\tau_{1,fit}(\delta) = A_3\delta^2 + B_3\delta + C_3 \tag{7.4}$$

$$\Delta\varepsilon_{2,fit}(\delta) = A_4\delta^2 + B_4\delta + C_4 \tag{7.5}$$

$$\tau_{2,fit}(\delta) = A_5\delta^2 + B_5\delta + C_5 \tag{7.6}$$

$$\sigma_{s,fit}(\delta) = A_6\delta^2 + B_6\delta + C_6 \tag{7.7}$$

Table 7.1. Temperature coefficients of the two-pole Cole-Cole model of temperature-dependent muscle mimicking phantom.

Parameter	n	A_n		B_n		C_n	
$\varepsilon'_{r\infty,fit}$	1	$0.6600 \cdot 10^{-3}$	K^{-2}	-0.1303	K^{-1}	8.2064	
$\Delta\varepsilon_{1,fit}$	2	$0.6464 \cdot 10^{-3}$	K^{-2}	-0.1293	K^{-1}	58.1866	
$\tau_{1,fit}$	3	5.4272	$\mathrm{fs{\cdot}K}^{-2}$	-0.5376	$\mathrm{ps{\cdot}K}^{-1}$	17.8300	ps
$\Delta\varepsilon_{2,fit}$	4	$-0.1804 \cdot 10^{-3}$	K^{-2}	0.0221	K^{-1}	58.6487	
$\tau_{2,fit}$	5	-0.1541	$\mathrm{ns{\cdot}K}^{-2}$	6.3925	$\mathrm{ns{\cdot}K}^{-1}$	438.3873	ns
$\sigma_{s,fit}$	6	$-0.1030 \cdot 10^{-3}$	$\mathrm{mS{\cdot}K}^{-2}$	0.0234	$\mathrm{mS{\cdot}K}^{-1}$	465.4264	mS

To quantify the accuracy of estimated Cole-Cole model i.e. fitting procedure, differences were analyzed between measured data and model. The difference was evaluated for both quantities over the frequency and temperature range as defined below.

$$\Delta\varepsilon'_{r,measured,fit}(\omega,\delta) = abs(\varepsilon'_{r,measured}(\omega,\delta) - \varepsilon'_{r,fit}(\omega,\delta)) \tag{7.8}$$

$$\Delta\sigma_{measured,fit}(\omega,\delta) = abs(\sigma_{measured}(\omega,\delta) - \sigma_{fit}(\omega,\delta)) \tag{7.9}$$

Detected differences were then illustrated by surface graphs 7.1, 7.2. Maximum, minimum and average differences for each temperature are indicated in Tabs. 7.2, 7.3. Deviations of relative permittivity are fluctuating over the frequency range, and overall are lower than 0.7. The average difference is increasing with temperature and is lower than 0.35. Electrical conductivity's average differences are almost identical over temperature range. However, the accuracy of the fitting procedure decreases with higher frequencies. The accuracy dependence corresponds to the one presented in [16].

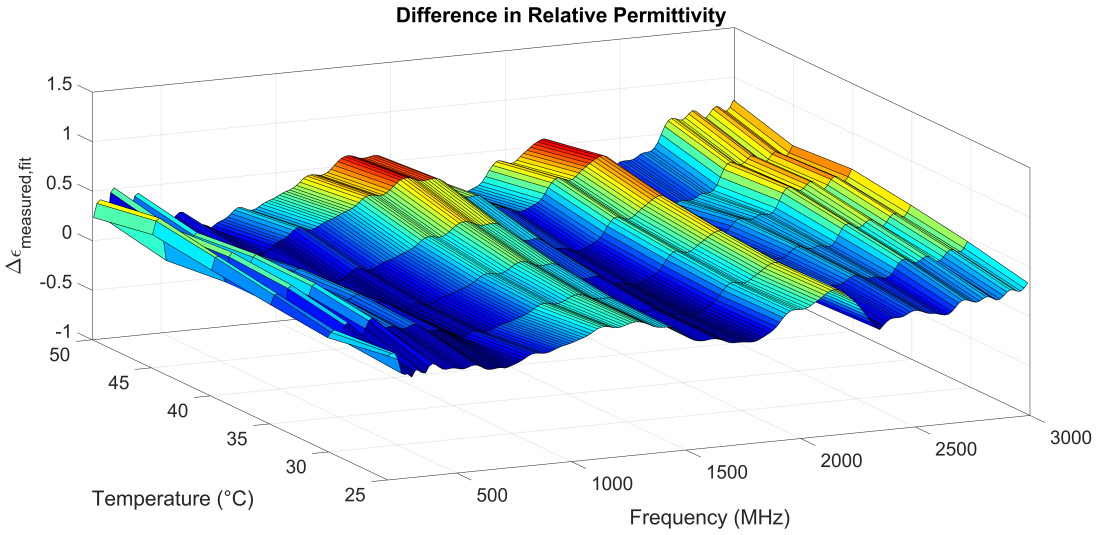

Figure 7.1. Differences between measured and fitted data by two-pole Cole-Cole model of relative permittivity.

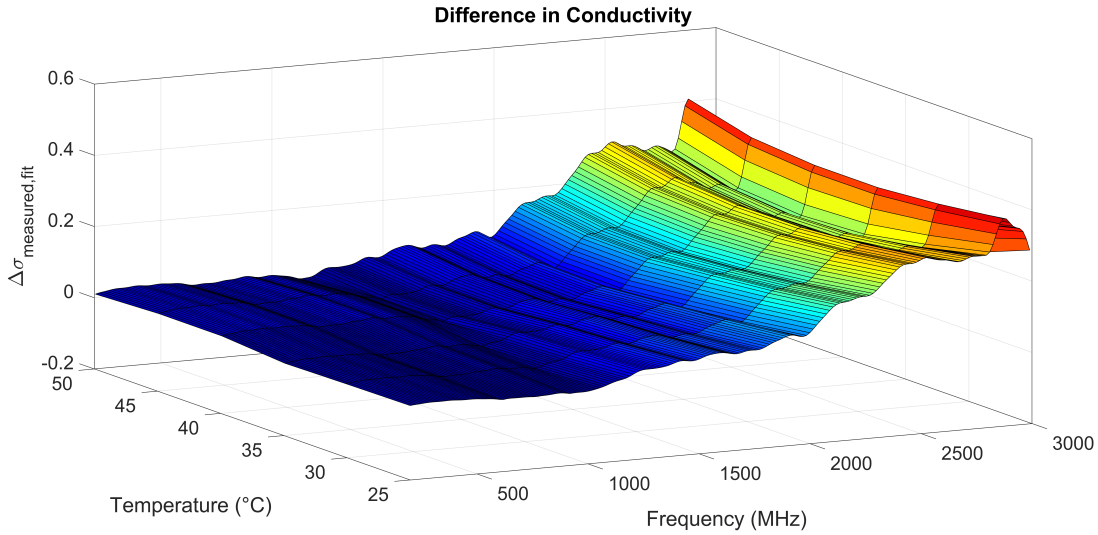

Figure 7.2. Differences between measured and fitted data by two-pole Cole-Cole model of conductivity.

Table 7.2. Absolute difference in relative permittivity $\Delta\varepsilon_{r,measured,fit}$ between the measurement and fitting procedure.

Temperature	Maximum	Minimum	Average
25 °C	0.46	10^{-3}	0.17
30 °C	0.46	10^{-3}	0.20
35 °C	0.56	10^{-3}	0.24
40 °C	0.64	10^{-3}	0.29
45 °C	0.69	10^{-3}	0.35
50 °C	0.77	10^{-3}	0.34

Table 7.3. Absolute difference in electrical conductivity $\Delta\sigma_{measured,fit}$ between the measurement and fitting procedure.

Temperature	Maximum	Minimum	Average
25 °C	0.38	10^{-4}	0.12
30 °C	0.36	10^{-4}	0.10
35 °C	0.35	10^{-4}	0.09
40 °C	0.35	10^{-4}	0.09
45 °C	0.36	10^{-4}	0.09
50 °C	0.41	10^{-4}	0.10

Figures 7.3, 7.4 present the temperature dependence of the dielectric properties of the phantom (dotted lines) along with its fitted model (solid lines). The intersection of the electrical conductivity of the model as well as the measurement is at the frequency point 2.41 GHz, whereas, Ley et al. observed this point at 3 GHz. The intersection point of the relative permittivity was observed at 6.5 GHz ([16]) which is out of this work's frequency range.

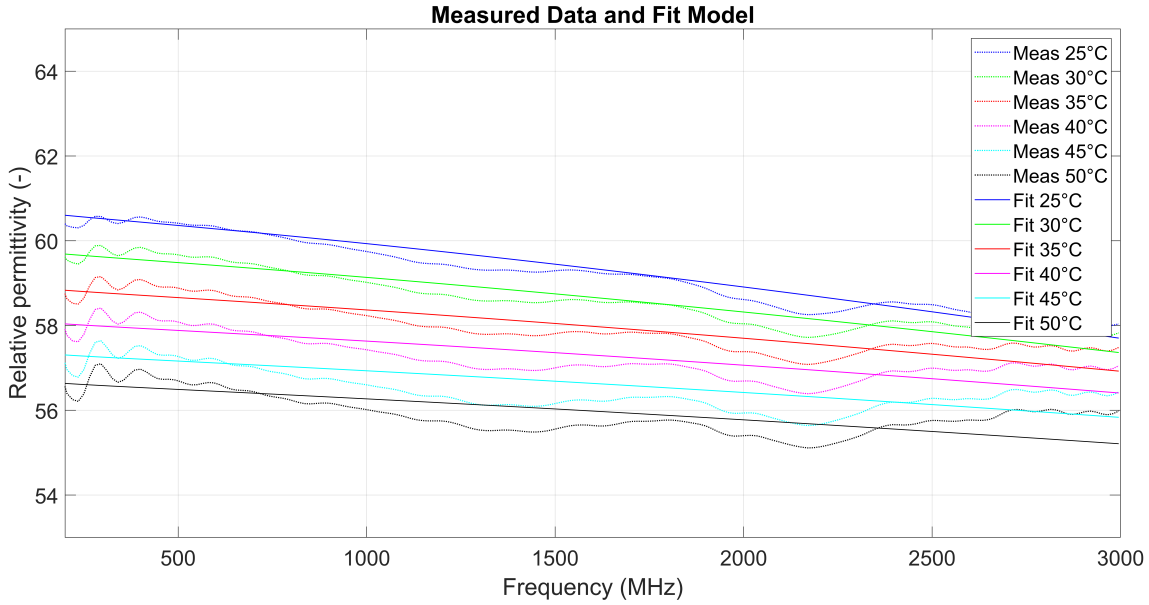

Figure 7.3. Measured relative permittivity along with Cole-Cole model.

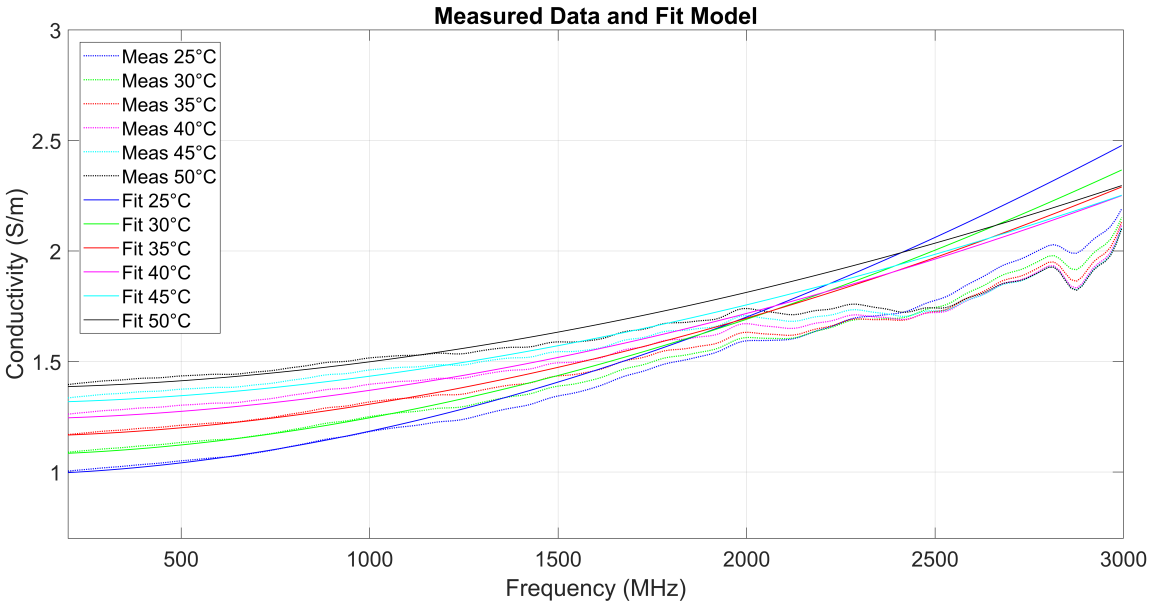

Figure 7.4. Measured conductivity along with Cole-Cole model.

Figures 7.5, 7.6 show the comparison of the two convenient phantoms (version 1 and 4) along with the references by Gabriel [15] and Ley [16]. The references differ from each other, especially for relative permittivity at lower frequencies. The firstly proposed phantom (version 1) has lower relative permittivity than the temperature-dependent one (version 4), however, the conductivity mimics Ley reference better. Generally, phantom's relative permittivity and conductivity for both versions vary less with the frequency than muscle tissue. Further investigation on broader frequency would be necessary. More studies are needed in order for accurate description of the biological tissues frequency dependence.

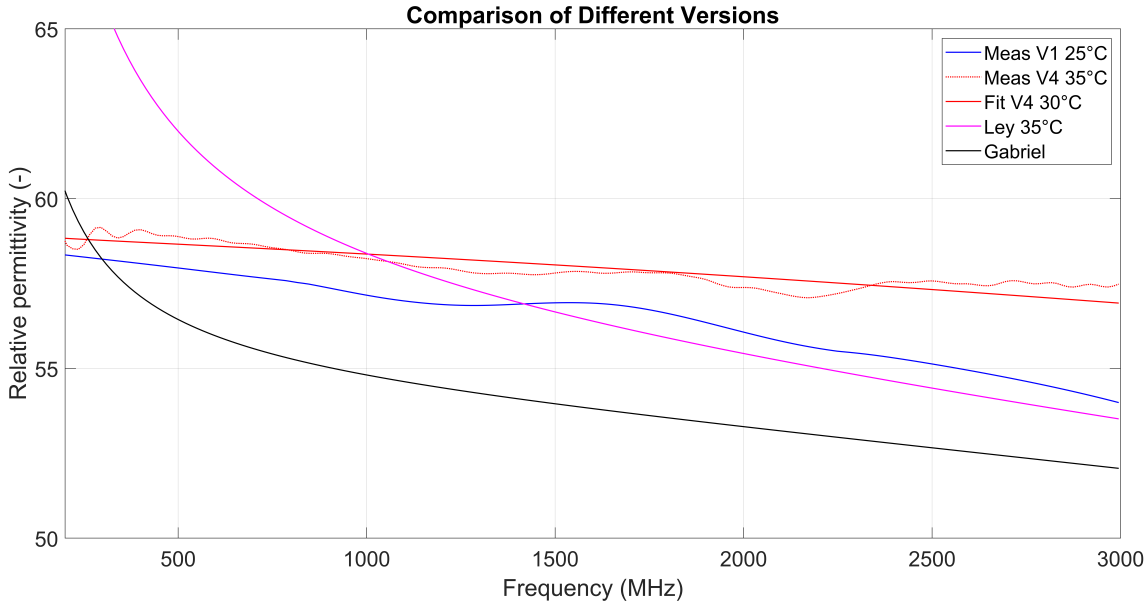

Figure 7.5. Comparison of relative permittivity of different proposed phantoms along with muscle references from Gabriel [15] and Ley [16].

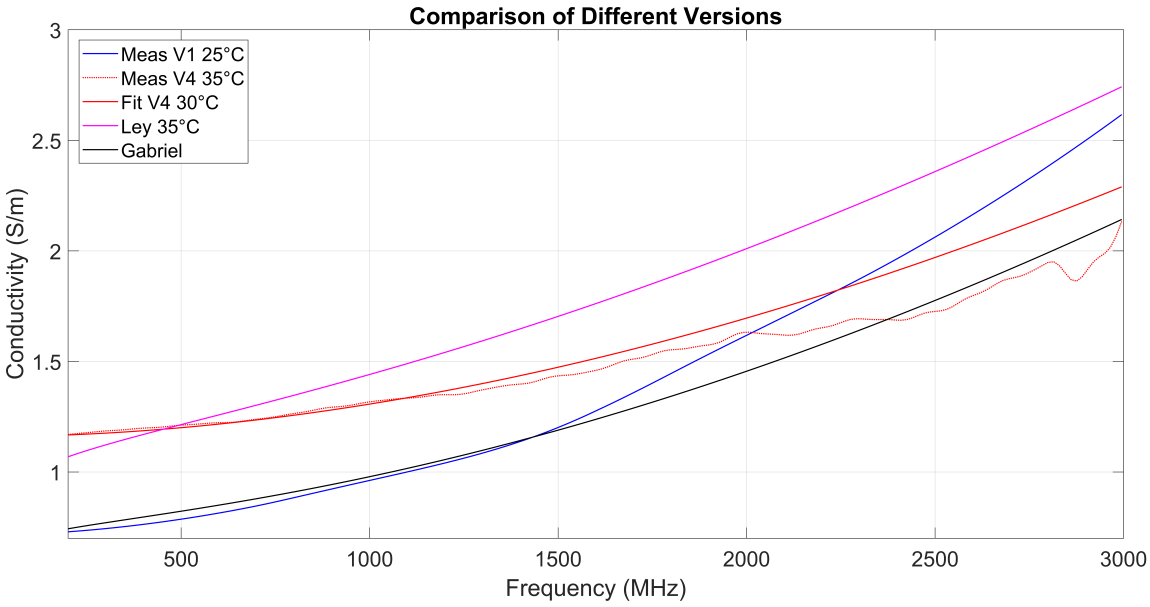

Figure 7.6. Comparison of different proposed phantoms' conductivity along with muscle references from Gabriel [15] and Ley [16].

Chapter 8
Tissue-Mimicking Phantom Fabrication

This chapter explains the fabrication procedure of the proposed phantom with great detail. Such description is necessary for reproducibility as well as for maintaining as identical results as possible. During phantom preparation, it is crucial to comply with the safety principles. Fabrication is easy and could be done with conventional equipment. However, some of the ingredients may cause health problems when not handled properly. The whole process is captured in appendix B.2.

Tools:

- Safety glasses mask, and gloves
- Precision laboratory scales
- Temperature
- Mesh
- Laboratory spatula
- Laboratory beakers app. volume 700 ml
- Induction cooker/gas burner/hot plate
- Steel pot
- Vacuum system

Phantom fabrication:

All ingredients were weight out on high-precision laboratory scales according to the table 8.1. With these weights, it is possible to prepare, for example, a phantom in the form of a cylinder with height 4.5 cm and a diameter of 9.2 cm (volume 299 cm^3). The mixture of powders consisting of TX-151 powder, agar powder and sodium chloride was prepared. The mixture of powders was gradually sprinkled to the distilled water by using a mesh and mix quickly. Gradual sprinkling over the mesh is necessary in order to obtain a smooth mixture without any lumps. The mask, gloves and safety glasses should be worn during the whole fabrication. The mixture is heated up to 85 °C (constant stirring of solution), which leads to the agar being solidified. The heater was switched to lower power when required consistency was reached. Polyethene powder was added and quickly mixed into the liquid. The mixture should be stirred long enough to make the PE powder being mixed properly and visually uniformly. The liquid was poured into the beaker (in this case in 700 ml beaker) and immediately put into the vacuum system. Vacuum system (approx. 0.6 bars due to the solidness of phantom) is used several times to remove air bubbles from the mixture, as shown in the 8.3, 8.4. It is necessary to place mixture in a vacuum system as soon as possible to get the least remaining air bubbles. When the phantom is solid, it is covered and kept at room temperature. Phantoms appeared to be pink material in a form matching the form of the beaker. The whole fabrication procedure took about 1 hour. The colour corresponds to TX-151 colour (there are also other TX-151 colour options). Consistency depends on the amount of PE powder, TX-151 and water.

The phantom does not change parameters for over a week but for longer preservation is possible to use a preservative. The dimensions of the phantom should be sufficiently big to avoid disturbing reflections.

Table 8.1. Composition of proposed muscle equivalent phantoms.

Ingredients	Version 1	Version 4
Distilled water (g)	300	335
Polyethylene powder (g)	49	40
TX-151 (g)	11	13
Agar powder (g)	9.2	9.2
Sodium chloride (g)	1.2	2.2

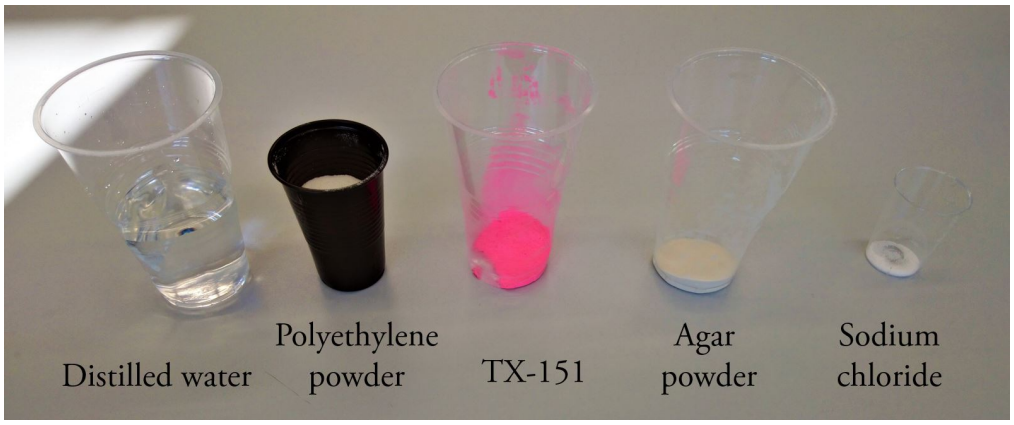

Figure 8.1. Photo of the ingredients used for fabrication.

Figure 8.2. Phantom placed in vacuum system.

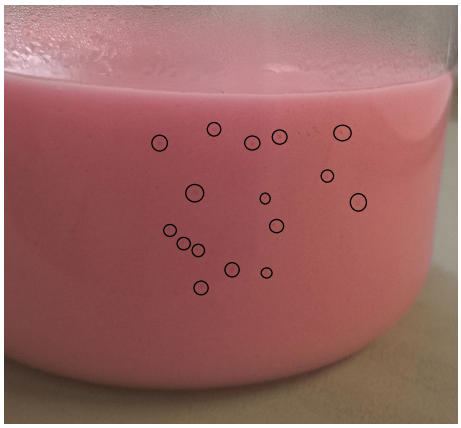

Figure 8.3. Detail of the mixture with marked out air bubbles right after preparation.

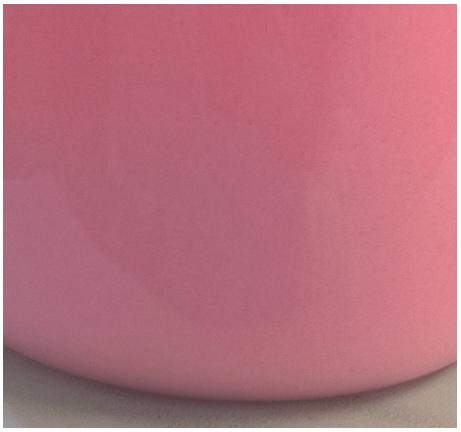

Figure 8.4. Detail of the result mixture after using vacuum system.

Figure 8.5. Photo of the prepared phantom in a cylindrical form.

Chapter 9
Conclusion

In this work, high-water content muscle mimicking phantom was designed for testing microwave imaging and hyperthermia systems. The phantom is intended for testing novel non-invasive temperature monitoring system via UWB radar in conjunction with hyperthermia system up to 50 °C. The proposed phantoms were designed to meet frequency, temperature and mechanical requirements. The final material is suitable for hyperthermia applications at ISM frequencies from 434 MHz to 2.45 GHz. The firstly proposed phantom for testing at the room temperature was presented on the conference IUPESM 2018 [5]. Phantom temperature measurement was presented at EuMCE 2019 in cooperation with TU Ilmenau [6]. The phantom suitable for temperature dependent measurements will be introduced in International Journal of Microwave and Wireless Technologies in 2020.

Overall more than 25 different phantom versions were prepared and only the best ones were presented in this work. Particular relative permittivity and conductivity values were achieved by gradual modification of the composition; consideration was also given to the consistency of the final phantom. The relative permittivity is mainly influenced by the proportion of water and polyethylene powder, while conductivity depends on sodium chloride. The procedure of preparation requires a vacuum system for removing any remaining air bubbles in the sample. The fabrication is simple and requires almost no special laboratory equipment. The detailed preparation process, along with the exact compositions is given in chapter 8. The dielectric properties were measured over a week, and no major changes were recorded even without using preservatives.

Possibility of replacing PE powder with sugar and honey was also investigated and the measured data shows that this substitution is not sufficient. However, this material may be used for a rough approximation due to its advantages: low cost; it is non-toxic, readily available material and ease of preparation. The best approximation is a sample consisting of 60% water, 31.4% grape sugar, 7% agar powder and 0.6% sodium chloride. With a higher percentage of the grape sugar and the use of TX-151 for consistency, there is also a risk of residual air bubbles in the sample.

The phantom composition of phantom suitable for testing at the room temperature (version 1) was then changed in order to obtain a temperature dependency which mimics muscle tissue. The adjustment was done mainly by the change of distilled water and PE powder composition, also the percentage of TX-151 was increased in order to get better mechanical properties and three consequent versions were prepared and tested. Temperature-dependent dielectric spectroscopy method presented in contribution [6] was used to improve the accuracy and to suppress the uncertainty of open-ended coaxial probe measurement. The phantom was heated from temperature 25 °C up to 50 °C with 5 °C step, the difference in relative permittivity and conductivity was then evaluated between each temperature step, which is crucial indicator of phantom's temperature behaviour considered in this work. The results were compared to the reference with the most recent temperature dependence of biological tissues by Ley et al. [16].

Two-pole Cole-Cole model which is temperature dependent was modelled for the best phantom referred as version 4. The average deviation of measurement compared to the model was around 0.27 for relative permittivity and 0.1 S/m for conductivity, which shows good accuracy of fitting procedure. Two phantoms with different proportion of composition were proposed for testing MW systems up to 3 GHz. The first version is appropriate for the measurements at room temperature and corresponds to the reference [15]. The second phantom is intended for differential temperature measurement and corresponds to ref.[16]. The compositions of both versions are summarised in the Tab. 9.1.

Table 9.1. Composition of proposed muscle equivalent phantom.

	Phantom acc [15]	Phantom acc [16]
Distilled water (%)	81.00	83.88
Polyethylene powder (%)	13.23	10.02
TX-151 (%)	2.97	3.25
Agar powder (%)	2.48	2.30
Sodium chloride (%)	0.32	0.55

References

[1] Organization, World Health. *Top 10 causes of death.* https://www.who.int/.

[2] Office, Czech Statistical. *Czech Statistical Office.* https://www.czso.cz/.

[3] Vrba, Jan. *Medical Applications of Microwaves*. 1. ed. Prague: Czech Technical University in Prague, 2003. ISBN 8001027058;9788001027059;.

[4] Fiser, Ondrej. *Microwave Hyperthermia for Treatment of Head and Neck Tumors Controlled by Non-Invasive Temperature Monitoring Based on UWB Radar*. Czech Technical University in Prague, 2018. Dissertation. http://hdl.handle.net/10467/75645.

[5] Kantova, M., O. Fiser, I. Merunka, J. Vrba, and J. Tesarik. High-water content phantom for microwave imaging and microwave hyperthermia. In: *IFMBE Proceedings*. Singapore: Springer, Singapore, 2019. ISSN 16800737. https://doi.org/10.1007/978-981-10-9023-3_141.

[6] Fiser, O, S Ley, M Helbig, J Sachs, M Kantova, and J Vrba. Temperature Dependent Dielectric Spectroscopy of Muscle Tissue Phantom. In: *2019 European Microwave Conference in Central Europe (EuMCE)*. 2019. pp. 550–553.

[7] Mayer, Daniel. *Aplikovaný elektromagnetizmus: úvod do makroskopické teorie elektromagnetického pole pro elektrotechnické inženýry*. České Budějovice: Kopp, 2012. ISBN 8072324365;9788072324361;.

[8] Balanis, Constantine A. *Advanced engineering electromagnetics*. John Wiley & Sons, 1999. ISBN 8126518561.

[9] Kittel, Charles. *Introduction to solid state physics*. 2nd ed. New York U6: Wiley, 1956.

[10] Technologies, Keysight. *Basics of Measuring the Dielectric Properties of Materials, Application Note.* http://literature.cdn.keysight.com/litweb/pdf/5989-2589EN.pdf.

[11] Schwan, H P, and K R Foster. RF-field interactions with biological systems: Electrical properties and biophysical mechanisms. *Proceedings of the IEEE*. 1980, Vol. 68, No. 1, pp. 104–113. ISSN 1558-2256 VO - 68. Available from DOI 10.1109/PROC.1980.11589.

[12] Cole, Kenneth S, and Robert H Cole. Dispersion and Absorption in Dielectrics I. Alternating Current Characteristics. *The Journal of Chemical Physics*. American Institute of Physics, apr, 1941, Vol. 9, No. 4, pp. 341–351. ISSN 0021-9606. Available from DOI 10.1063/1.1750906. https://doi.org/10.1063/1.1750906.

[13] Raju, Gorur Govinda. *Dielectric Loss and Relaxation—I*. Available from DOI 10.1201/b20223-4. https://www.routledgehandbooks.com/doi/10.1201/b20223-4.

[14] Cole, Kenneth S, and Robert H Cole. *Dispersion and Absorption in Dielectrics II. Direct Current Characteristics*. Available from DOI 10.1063/1.1723677.

[15] Gabriel, S, R W Lau, and C Gabriel. The dielectric properties of biological tissues: III. Parametric models for the dielectric spectrum of tissues. *Physics in Medicine and Biology*. nov, 1996, Vol. 41, No. 11, pp. 2271–2293. ISSN 0031-9155. Available from DOI 10.1088/0031-9155/41/11/003.

[16] Ley, Sebastian, Susanne Schilling, Ondrej Fiser, Jan Vrba, Jürgen Sachs, and Marko Helbig. *Ultra-Wideband Temperature Dependent Dielectric Spectroscopy of Porcine Tissue and Blood in the Microwave Frequency Range*. Available from DOI 10.3390/s19071707.

[17] Gregory, A P, and R N Clarke. A review of RF and microwave techniques for dielectric measurements on polar liquids. *IEEE Transactions on Dielectrics and Electrical Insulation*. 2006, Vol. 13, No. 4, pp. 727–743. ISSN 1558-4135 VO - 13. Available from DOI 10.1109/TDEI.2006.1667730.

[18] Dabbagh, Ali, Basri Johan Jeet Abdullah, Chanthiriga Ramasindarum, and Noor Hayaty Abu Kasim. Tissue-Mimicking Gel Phantoms for Thermal Therapy Studies. *Ultrasonic Imaging*. 2014, Vol. 36, No. 4, pp. 291–316. Available from DOI 10.1177/0161734614526372.
https://doi.org/10.1177/0161734614526372.

[19] P.Hasgall, E.Neufeld, M.Gosselin, A.Klingenböck, and N.Kuster. *IT'IS database for thermal and electromagnetic parameters of biological tissues*. Available from DOI 10.13099/VIP21000-03-1.
www.itis.ethz.ch/database.

[20] Culjat, M, D Goldenberg, and P Tewari. A Review of Tissue Substitutes for Ultrasound Imaging. *Ultrasound in medicine & biology*. jun, 2010, Vol. 36, pp. 861–873. Available from DOI 10.1016/j.ultrasmedbio.2010.02.012.

[21] McDermott, B., B. McGinley, K. Krukiewicz, B. Divilly, M. Jones, M. Biggs, M. O'Halloran, and E. Porter. Stable tissue-mimicking materials and an anatomically realistic, adjustable head phantom for electrical impedance tomography. *Biomedical Physics & Engineering Express*. IOP Publishing, 2017, Vol. 4, No. 1, pp. 15003. Available from DOI 10.1088/2057-1976/aa922d.

[22] Liu, Yunbo, Brady Connors, Monica Abboud, and Subha Maruvada. Egg white-based ultrasound blood mimicking phantom. *The Journal of the Acoustical Society of America*. Acoustical Society of America, mar, 2019, Vol. 145, No. 3, pp. 1922. ISSN 0001-4966. Available from DOI 10.1121/1.5101980.
https://doi.org/10.1121/1.5101980.

[23] Garrett, J, and E Fear. Stable and Flexible Materials to Mimic the Dielectric Properties of Human Soft Tissues. *IEEE Antennas and Wireless Propagation Letters*. 2014, Vol. 13, pp. 599–602. ISSN 1548-5757 VO - 13. Available from DOI 10.1109/LAWP.2014.2312925.

[24] Garrett, J, and E Fear. A New Breast Phantom With a Durable Skin Layer for Microwave Breast Imaging. *IEEE Transactions on Antennas and Propagation*. 2015, Vol. 63, No. 4, pp. 1693–1700. ISSN 1558-2221 VO - 63. Available from DOI 10.1109/TAP.2015.2393854.

[25] Pokorny, Tomas, D Vrba, Jan Tesarik, and Dario Rodrigues. Anatomically and Dielectrically Realistic 2.5D 5-Layer Reconfigurable Head Phantom for Testing Microwave Stroke Detection and Classification. *International Journal of*

Antennas and Propagation. aug, 2019, Vol. 2019, pp. 1–7. Available from DOI 10.1155/2019/5459391.

[26] McDermott, B., E. Porter, M. O'Halloran, A. Poudel, M. Biggs, N. S. Karode, and A. B. Coffey. 3D Printable Solid Tissue-Mimicking Material for Microwave Phantoms. In: *2018 EMF-Med 1st World Conference on Biomedical Applications of Electromagnetic Fields (EMF-Med)*. 2018. pp. 1–2. Available from DOI 10.23919/EMF-MED.2018.8526005.

[27] Lazebnik, M., E. L. Madsen, G. R Frank, and S. C Hagness. Tissue-mimicking phantom materials for narrowband and ultrawideband microwave applications. *Physics in Medicine and Biology*. sep, 2005, Vol. 50, No. 18, pp. 4245–4258. ISSN 0031-9155. Available from DOI 10.1088/0031-9155/50/18/001.

[28] Guy, Arthur W. Analyses of Electromagnetic Fields Induced in Biological Tissues by Thermographic Studies on Equivalent Phantom Models. *IEEE Transactions on Microwave Theory and Techniques*. 1968. ISSN 15579670. Available from DOI 10.1109/TMTT.1968.1127484.

[29] Koopman, David W. Experimental Development of Simulated Biomaterials for Dosimetry Studies of Hazardous Microwave Radiation. *IEEE Transactions on Microwave Theory and Techniques*. 1976. ISSN 15579670. Available from DOI 10.1109/TMTT.1976.1128936.

[30] Lagendijk, J J W, and P Nilsson. Hyperthermia dough: a fat and bone equivalent phantom to test microwave/radiofrequency hyperthermia heating systems. *Physics in Medicine and Biology*. jul, 1985, Vol. 30, No. 7, pp. 709–712. ISSN 0031-9155. Available from DOI 10.1088/0031-9155/30/7/011.

[31] Maneas, Efthymios, Wenfeng Xia, Olumide Ogunlade, Martina Fonseca, Daniil I Nikitichev, Anna L David, Simeon J West, Sebastien Ourselin, Jeremy C Hebden, Tom Vercauteren, and Adrien E Desjardins. Gel wax-based tissue-mimicking phantoms for multispectral photoacoustic imaging. *Biomed. Opt. Express*. OSA, 2018, Vol. 9, No. 3, pp. 1151–1163. Available from DOI 10.1364/BOE.9.001151.
http://www.osapublishing.org/boe/abstract.cfm?URI=boe-9-3-1151.

[32] Negussie, Ayele H, Ari Partanen, Andrew S Mikhail, Sheng Xu, Nadine Abi-Jaoudeh, Subha Maruvada, and Bradford J Wood. Thermochromic tissue-mimicking phantom for optimisation of thermal tumour ablation.. *International Journal of Hyperthermia*. Taylor & Francis Ltd, may, 2016, Vol. 32, No. 3, pp. 239–243. ISSN 02656736.
http://10.0.12.37/02656736.2016.1145745.

[33] Eranki, Avinash, Andrew S Mikhail, Ayele H Negussie, Prateek S Katti, Bradford J Wood, and Ari Partanen. Tissue-mimicking thermochromic phantom for characterization of HIFU devices and applications. *International Journal of Hyperthermia*. Taylor & Francis, jan, 2019, Vol. 36, No. 1, pp. 518–529. ISSN 0265-6736. Available from DOI 10.1080/02656736.2019.1605458.

[34] Joachimowicz, N, C Conessa, T Henriksson, and B Duchêne. Breast Phantoms for Microwave Imaging. *IEEE Antennas and Wireless Propagation Letters*. 2014, Vol. 13, pp. 1333–1336. ISSN 1548-5757 VO - 13. Available from DOI 10.1109/LAWP.2014.2336373.

[35] Joachimowicz, Nadine, Bernard Duchêne, Christophe Conessa, and Olivier Meyer. *Anthropomorphic Breast and Head Phantoms for Microwave Imaging*. Available from DOI 10.3390/diagnostics8040085.

[36] Pollacco, D A, M Caligari Conti, L Farrugia, P Schembri Wismayer, L Farina, and C V Sammut. Dielectric properties of muscle and adipose tissue-mimicking solutions for microwave medical imaging applications. *Physics in Medicine & Biology*. IOP Publishing, 2019, Vol. 64, No. 9, pp. 95009. ISSN 1361-6560. Available from DOI 10.1088/1361-6560/ab0dda.
http://dx.doi.org/10.1088/1361-6560/ab0dda.

[37] Britannica, Encyclopædia. *Ringer's solution*.
academic-eb-com . ezproxy . techlib . cz / levels / collegiate / article / Ringers-solution/63724.

[38] Di Meo, Simona, Lorenzo Pasotti, Ioannis Iliopoulos, Marco Pasian, Mauro Ettorre, Maxim Zhadobov, and Giulia Matrone. Tissue-mimicking materials for breast phantoms up to 50 GHz. *Physics in Medicine & Biology*. IOP Publishing, 2019, Vol. 64, No. 5, pp. 55006. ISSN 1361-6560. Available from DOI 10.1088/1361-6560/aafeec.

[39] Britannica, Encyclopædia. *agar*.
academic-eb-com.ezproxy.techlib.cz/levels/collegiate/article/agar/3986.

[40] Józefczak, A, K Kaczmarek, M Kubovčíková, Z Rozynek, and T Hornowski. The effect of magnetic nanoparticles on the acoustic properties of tissue-mimicking agar-gel phantoms. *Journal of Magnetism and Magnetic Materials*. 2017, Vol. 431, pp. 172–175. ISSN 0304-8853. Available from DOI https://doi.org/10.1016/j.jmmm.2016.09.118.
http://www.sciencedirect.com/science/article/pii/S0304885316323514.

[41] Ishida, T, and H Kato. Muscle Equivalent Agar Phantom for 13.56MHz RF-Induced Hyperthermia. *Shimane journal of medical science*. Shimane University, 1980, Vol. 4, No. 2, pp. 134–140. ISSN 03865959.
http://ci.nii.ac.jp/naid/110000012588/en/.

[42] Kato, Hirokazu, Masahiro Hiraoka, and Tetsuya Ishida. An agar phantom for hyperthermia. *Medical Physics*. American Association of Physicists in Medicine, 1986, Vol. 13, No. 3, pp. 396–398. ISSN 2473-4209. Available from DOI 10.1118/1.595882.
http://dx.doi.org/10.1118/1.595882.

[43] Kato, H, and T Ishida. Development of an agar phantom adaptable for simulation of various tissues in the range 5-40 MHz. (Hyperthermia treatment of cancer). *Physics in Medicine and Biology*. feb, 1987, Vol. 32, No. 2, pp. 221–226. ISSN 0031-9155. Available from DOI 10.1088/0031-9155/32/2/006.

[44] Ito, K, K Furuya, Y Okano, and L Hamada. Development and characteristics of a biological tissue-equivalent phantom for microwaves. *Electronics and Communications in Japan (Part I: Communications)*. John Wiley & Sons, Inc., 2001, Vol. 84, No. 4, pp. 67–77. ISSN 1520-6424. Available from DOI 10.1002/1520-6424(200104)84:4¡67::AID-ECJA8¿3.0.CO;2-D.

[45] Onishi, Teruo, Ryo Ishido, Takuya Takimoto, Kazuyuki Saito, Shinji Uebayashi, Masaharu Takahashi, and Koichi Ito. Biological tissue-equivalent agar-based solid phantoms and SAR estimation using the thermographic method in the range of 3-6 GHz. *IEICE Transactions on Communications*. 2005. ISSN 17451345. Available from DOI 10.1093/ietcom/e88-b.9.3733.

[46] Chen, Heng-Yin, and Nelson G Chen. Spectrophotometric and thermal stability of agarose-based ultrasonic tissue-mimicking gel. *Journal of Applied Physics*.

American Institute of Physics, apr, 2019, Vol. 125, No. 15, pp. 155104. ISSN 0021-8979. Available from DOI 10.1063/1.5082822.

[47] Souza, R.M., R.M. Monteiro, R. P.B. Costa-Felix, and A.V. Alvarenga. Ultrasonic properties of a four years old tissue-mimicking material. *Journal of Physics: Conference Series*. IOP Publishing, 2018, Vol. 975, pp. 12025. ISSN 1742-6588. Available from DOI 10.1088/1742-6596/975/1/012025. http://dx.doi.org/10.1088/1742-6596/975/1/012025.

[48] Mobashsher, A T, and A M Abbosh. Artificial Human Phantoms: Human Proxy in Testing Microwave Apparatuses That Have Electromagnetic Interaction with the Human Body. *IEEE Microwave Magazine*. 2015, Vol. 16, No. 6, pp. 42–62. ISSN 1557-9581 VO - 16. Available from DOI 10.1109/MMM.2015.2419772.

[49] Jilani, Muhammad Taha. A Brief Review of Measuring Techniques for Characterization of Dielectric Materials. *International Journal of Information Technology and Electrical Engineering*. dec, 2012.

[50] Fenske, K, and D Misra. Dielectric materials at microwave frequencies. *Applied Microwave and Wireless*. oct, 2000, Vol. 12, pp. 92–100.

[51] Zajicek, R., L. Oppl, and J. Vrba. Broadband Measurement of Complex Permittivity Using Reflection Method and Coaxial Probes. *Radioengineering*. 2008, Vol. 17, pp. 14–19. http://hdl.handle.net/11012/57173.

[52] Lazebnik, Mariya, Mark C Converse, John H Booske, and Susan C Hagness. Ultrawideband temperature-dependent dielectric properties of animal liver tissue in the microwave frequency range. *Physics in Medicine and Biology*. apr, 2006, Vol. 51, No. 7, pp. 1941–1955. ISSN 0031-9155. Available from DOI 10.1088/0031-9155/51/7/022.

[53] Ley, Sebastian, Ondrej Fiser, Ilja Merunka, Jan Vrba, J Sachs, and M Helbig. *Preliminary Investigations for Reliable Temperature Dependent UWB Dielectric Spectroscopy of Tissues and Tissue Mimicking Phantom Materials*. 2018. Available from DOI 10.1049/cp.2018.0789.

Appendix A
Abbreviations and Symbols

A.1 List of Abbreviations

ABS	Acrylonitrile butadiene styrene
BSA	Bovine serum albumin
EIT	Electric impedance tomography
EM	Electro–magnetic
HIFU	High intensity focused ultrasound
MRI	Magnetic resonance imaging
MUT	Material under test
MW	Microwave
PBS	Phosphate buffered saline
PVC	Polyvinyl chloride
SEBS	Poly(styrene-b-ethylene-butylene-b-styrene)
TE	Transverse electric
TM	Transverse magnetic
TEM	Transverse electro-magnetic
T-M	Tissue-mimicking
TMM	Tissue-mimicking material
TX-100	Triton X-100
VNA	Vector network analyzer

A.2 List of Symbols

Symbol	Unit	Quantity
δ	°C	temperature
ε	F/m	permittivity
$\varepsilon*$	-	complex permittivity
ε'	-	real part of permittivity
ε''	-	imaginary part of permittivity
ε_0	F/m	vacuum permittivity
ε_r	-	relative permittivity
$\varepsilon_{r,s}$	-	ε' at zero frequency
$\varepsilon_{r,\infty}$	-	ε' at infinite frequency
$\varkappa$	-	electrical susceptibility
Γ	-	reflection coefficient
λ	m	wavelength
μ_e	$m^2/(V\cdot s)$	electron mobility
μ	H/m	permeability
μ_r	-	relative permeability
ρ	C/m^2	electric charge density
σ	S/m	electrical conductivity
σ_a	S/m	alternating field conductivity
σ_s	S/m	static conductivity
τ	s	relaxation time
τ_e	s	new relaxation time
ω	rad/s	angular frequency
$\boldsymbol{B}$	T	vector of magnetic induction
c	m/s	speed of light
$\boldsymbol{D}$	$C\cdot m^{-2}$	vector of electric displacement field
$\boldsymbol{E}$	N/C	vector of electric field intensity
f	Hz	frequency
$\boldsymbol{H}$	A/m	vector of magnetic field intensity
k_0	1/m	free-space number of EM wave
J_v	A/m^2	electric current density
$\boldsymbol{P}$	C/m^2	electric polarization
q_{ve}	$C\cdot m^{-3}$	electron charge density
$\boldsymbol{p_t}$	C · m	total dipole moment
t	s	time
v	m/s	velocity
Z	Ω	impedance

Appendix B
Additional Figures and Photos

B.1 Additional Figures

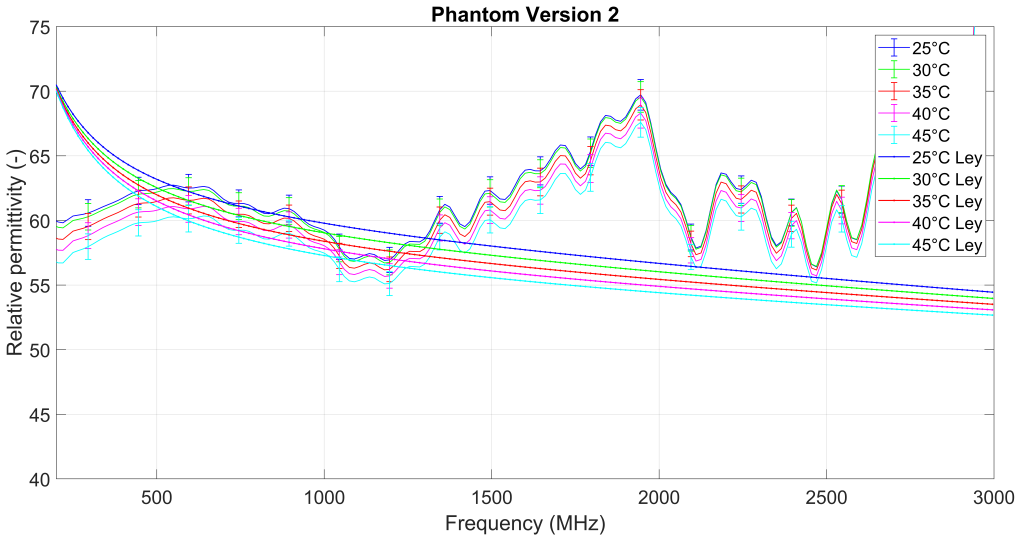

Figure B.1. Relative permittivity's temperature dependence of phantom version 2 along with temperature dependence of muscle tissue according to Ley et al. [16].

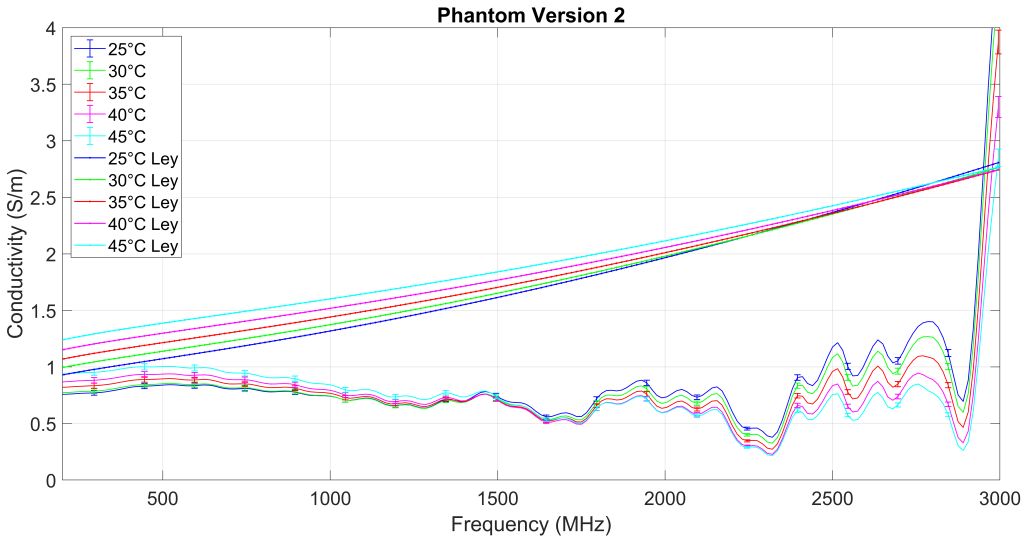

Figure B.2. Temperature dependence of electrical conductivity of phantom version 2 along with temperature dependence of muscle tissue according to Ley et al. [16].

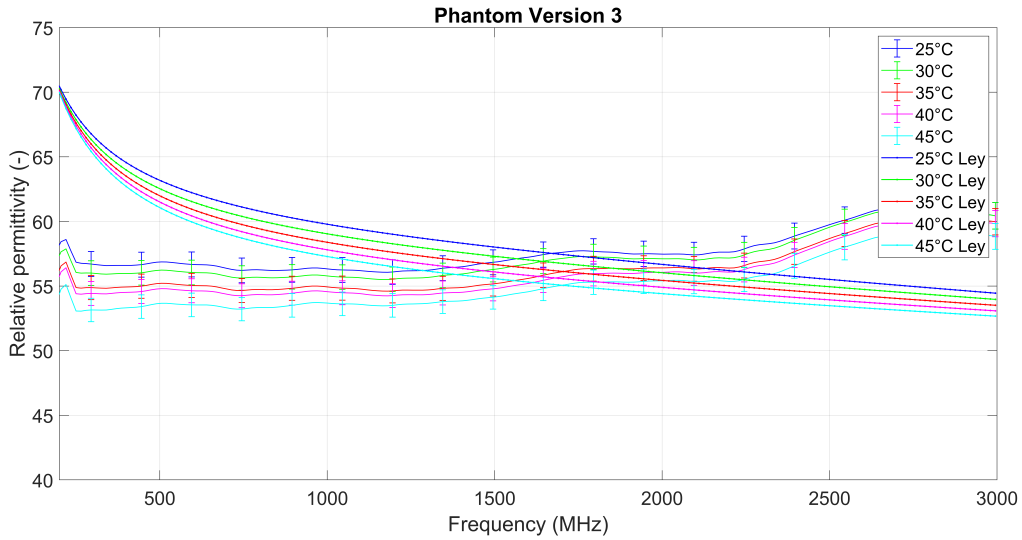

Figure B.3. Relative permittivity's temperature dependence of phantom version 3 along with temperature dependence of muscle tissue according to Ley et al. [16].

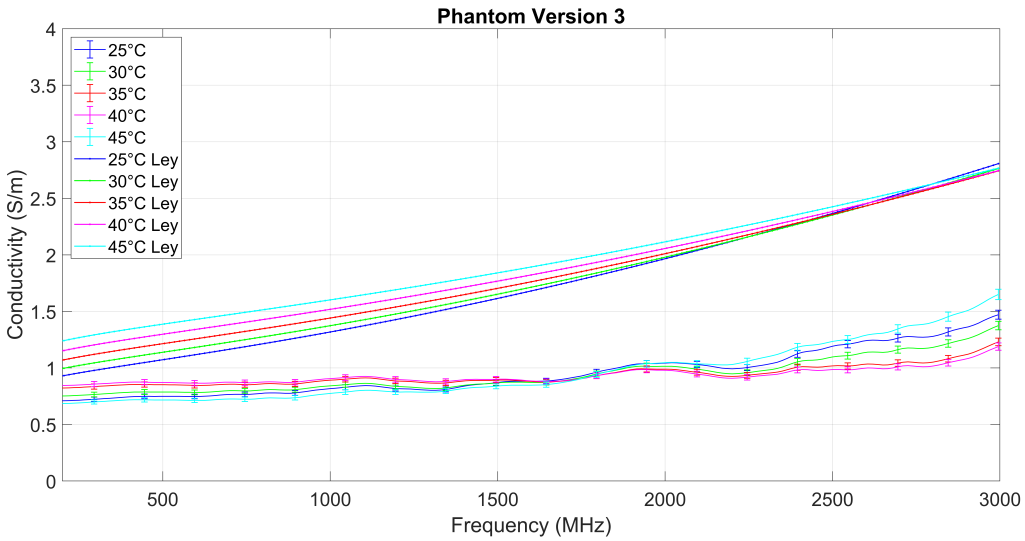

Figure B.4. Temperature dependence of electrical conductivity of phantom version 3 along with temperature dependence of muscle tissue according to Ley et al. [16].

B.2 Pictures of Preparation of Tissue-Mimicking Material

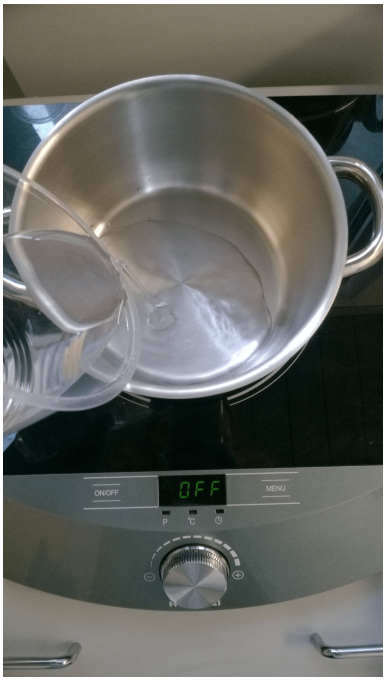

Figure B.5. Pouring distilled water.

Figure B.6. Dissolving sodium chloride.

Figure B.7. Sprinkling of the mixture of powders.

Figure B.8. Warming the mixture.

Figure B.9. At temperature above 85 °C, agar solidify and PE powder can be mixed in.

Figure B.10. Sprinkling and mixing polyethylene powder.

Figure B.11. Use of vacuum system to remove air bubbles from the mixture.

Figure B.12. Letting mixture to cool down.